INITIAL WAVES FROM DEFORMABLE SUBMARINE LANDSLIDES

A STUDY ON THE SEPARATION TIME AND PARAMETER RELATIONSHIPS

A Thesis

by

JUSTIN ANDREW O'SHAY

Submitted to the Office of Graduate Studies of
Texas A&M University
in partial fulfillment of the requirements for the degree of

MASTER OF SCIENCE

May 2012

Major Subject: Geophysics

INITIAL WAVES FROM DEFORMABLE SUBMARINE LANDSLIDES

A STUDY ON THE SEPARATION TIME AND PARAMETER RELATIONSHIPS

A Thesis

by

JUSTIN ANDREW O'SHAY

Submitted to the Office of Graduate Studies of
Texas A&M University
in partial fulfillment of the requirements for the degree of

MASTER OF SCIENCE

Approved by:

Chair of Committee,	Robert Weiss
	David Sparks
Committee Members,	James Kaihatu
Head of Department,	Rick Giardino

May 2012

Major Subject: Geophysics

ABSTRACT

Initial Waves from Deformable Submarine Landslides
A Study on the Separation Time and Parameter Relationships. (May 2012)
Justin Andrew O'Shay, B.S., Texas A&M University
Chair of Advisory Committee: Dr. Robert Weiss
Dr. David Sparks

Earthquake and submarine mass failure are the most frequent causes of tsunami waves. While the process of the tsunami generation by earthquakes is reasonably well understood, the generation of tsunami waves during submarine mass failure is not. Estimates of the energy released during a tsunamigenic earthquake and respective tsunami wave draw a clear picture of the efficiency of the tsunami-generating process. However for submarine landslides, this is not as straightforward because the generation process has never been recorded in nature making energy inferences very difficult. Hence the efficiency of submarine landslide as tsunami generators is yet to be conclusively determined. As the result of this uncertainty, different equations, derived from experimental data or theory, result in leading-wave amplitude that vary over 6 orders of magnitude for the same initial slide conditions. To arrive at more robust estimates of the leading-wave characteristics and associated runup, the spatiotemporal dynamics of the coupling between the slide body and water column needs to be investigated. The duration the water surface deformation is coupled with the slide motion is an essential question to shed light on the energy transfer. A parametric study is conducted with the state-of-the-art hydrocode iSALE in order to shed light on this complex geophysical event. The mass, viscosity, and depth

of submergence are the particular slide parameters varied and their relationship to runup and decoupling time is analyzed.

TABLE OF CONTENTS

Page

LIST OF TABLES

LIST OF FIGURES

FIGURE Page

FIGURE Page

FIGURE Page

1. INTRODUCTION

1.1 Introduction to tsunamis

The word tsunami was first used in the United States in 1896 in a National Geographic article describing the June 15, 1896 "great earthquake wave (tsunami)" that struck the coast of Hando, the main island of Japan, and killed over 25,000 people (Scidmore, 1896). The Japanese etymological roots for tsunami *tsu* and *nami* literally mean "harbor wave" and although this is not accurate, it is the generally accepted term to describe this event. Tidal wave, seismic sea wave, and earthquake wave are also used to some extent. These terms, with the exception of tidal wave, more literally describe the actual physics since the majority of these events are generated either directly or indirectly by co-seismic deformation of the seafloor.

Tsunamis are shallow water waves generated by impulsively driven geophysical events. They are called shallow water waves because they have a very long wave length and period compared to their height or amplitude. This ratio of length scales also causes the energy dissipation of these events to be very low as they travel. This in itself is the reason these waves are known for their ability to travel across an entire ocean and strike a distant coastline with enough energy to still cause catastrophic damage. Not only the scientific community but the general public has been galvanized recently by the event that occurred of the coast of Japan on March 11, 2011 and destroyed the Fukushima Nuclear Power Plant, McCurry (2011); Fujii et al. (2011), the 2004 Boxing Day event in the Indian Ocean, Geist et al. (2007), and the 1998 Papua New Guinea earthquake and tsunami (Asari et al., 2000; McSaveney et al., 2000). These events led to a rekindled focus on tsunami research and put a concentrated emphasis on the need to understand the risk and mitigate the damage that can be potentially caused.

This thesis follows the style of *Society of Exploration Geophysicists*.

In the past few decades tsunami research and modeling has made significant strides in understanding this complex phenomenon. Specific people include Ben-Menahem and Rosenman (1972) who made great strides in understanding the amplitude patterns that can be generated from different sources. Three separate papers by Ward (1980, 1981, 1982) analyzed tsunamigenesis in the near field from both a point source and line source and found evidence to support the critical effect of the seismic moment, depth of source, and generation mechanism. Okal (1988) who worked on the full cycle of these events, cited the importance of the directionality of the source mechanism and the importance that the bathymetric profile has on the far field amplitude along the propagation direction. Synolakis (1991) studied the difference between the linear theory and non linear theory when analyzing runup events and found that little difference existed in the difference between the two. Tadepalli and Synolakis further studied run-up and proposed the famous N-wave solution for modeling this behavior (Tadepalli and Synolakis, 1994). Tsunami research since the 1990's has also been marked by both the application of large scale numerical models, National Oceanic and Atmospheric Administration's (N.O.A.A.) use of the Method of Splitting Tsunami (M.O.S.T.) numerical model as a hazard mitigation tool see Titov and Gonzalez (1997), and post inundation field studies to get a better grasp of the costal effects of these events (Yeh et al., 1993; Satake et al., 1993; Synolakis et al., 1995; Tsuji et al., 1995; Bourgeois et al., 1999; Kawata et al., 1999; Weiss and Bahlburg, 2006; Goff et al., 2006; Borrero et al., 2006, 2009).

Impulsive events in or around the ocean can be tsunami generators. Known causes include earthquakes, landslides (both aerial or subaqueous), volcanic eruptions, submarine explosions, and bolide impacts. Historically the consensus has been that earthquakes account for the majority of the tsunamis generated worldwide. The 1998 Papua New Guinea event, however, has caused a portion of the scientific community to realize they need to reassess the destructive potential of this type of hazard. On March 7, 1998 a 7.0 magnitude earthquake struck 25 km off the coast of

Papua New Guinea causing submarine landslides and tsunami waves killing ≈ 2000 people. A number of researchers hold to the view that this event was largely tectonic in origin (e.g. Kikuchi et al. (1999); Matsuyama et al. (1999); Satake and Tanioka (2003); Tanioka (1999); Geist (2000, 2001)) while others believe that the amplitude of wave heights during the event is indicative of that of a landslide generated wave (Heinrich et al., 2000; Titov et al., 2001; Okal and Synolakis, 2001, 2003; Synolakis et al., 2002; Lynett et al., 2003; Okal, 2003). This was further backed up by the discovery of a large submarine landslide scarp found off the coast that was estimated to have occurred during the earthquake (Tappin et al., 2001). Regardless of the actual cause of this particular event, it undoubtedly acted as a catalyst for research into landslide induced wave phenomena and caused scientists to reanalyze past events looking to identify this hazard in the historical record. Up to this point, however, researchers have had great difficulty in accurately modeling this event, which unlike earthquake sourced events can be quite a "vexing problem" because of their near source destructive potential (Bardet et al., 2003).

1.2 Introduction to landslide-generated tsunamis

Described by Bardet et al. (2003) as "defying all analyses", landslide generated tsunamis are currently considered one of the most perplexing of the source mechanisms for tsunami generation. It was noted earlier that work in this area was catalyzed by the 1998 Papua New Guinea event, but it is important to note that the awareness of landslide generated tsunami waves goes back significantly farther than that. The earliest proposed account of this phenomena, to this authors knowledge, comes from Mallet's report to the British Association in 1858. He was quoted by Milne in 1898 in his famous text *Earthquakes and other Earth movements* as suggesting that water waves could be generated from the "underwater slippage" of material (Milne, 1898). Following this, de Ballore (1907) who quotes earlier work by Verbeck (1900) argues that the waves off the coast of Ceram in 1899 most likely

originated from a landslide since the origin of the earthquake was "incontestably tectonic and on land." Gutenberg (1939), using this work, states quite absolutely that submarine landslides "must produce tsunamis" and that this truth seems presently "unavoidable."

The concept of a landslide induced tsunami was quite silent until Ambraseys (1960) interpreted the 1956 tsunami at Amorgos, Greece as being caused by a series of submarine landslides, supporting earlier work by Galanopoulos (1956). Then in 1964 Alaska was struck by an earthquake which was believed to have caused large waves generated in the lakes and fjords from major landslides in the area (Plafker and Meyer, 1967). In the 1980s Hasegawa and Kanamori studied the 1929 Grand Banks, Alaska tsunami and Eissler and Kanamori the 1975 Kalapana, Hawaii event, finding both to have been generated by large submarine landslides induced by large earthquakes near the coast (Hasegawa and Kanamori, 1987; Eissler and Kanamori, 1987). In the last two decades a landslide source of the 1946 Aleutian tsunami has also been proposed, though with some debate (Kanamori, 1972; Pelayo and Wiens, 1992; Fryer et al., 2001; Okal et al., 2002, 2003; Fryer et al., 2004; Okal, 2004). Other examples include the 1992 Flores Indonesia and 1999 Izmit Turkey events which were noted to have a run up frequency distribution to support the influence of landslide events (Imamura et al., 1995; Altinok et al., 2001).

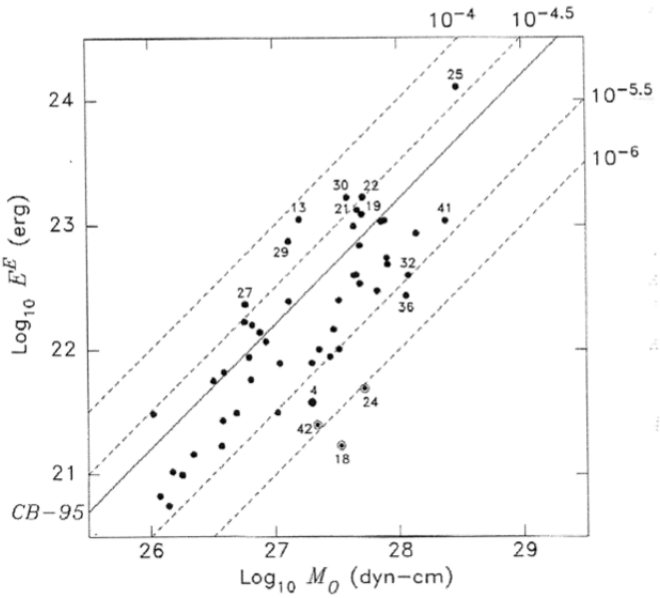

Fig. 1.1.: Estimated earthquake energy, E^E, compared to the earthquakes generating moment, M_0. The circled dots are those nicknamed "tsunami earthquakes" and can be determined by the two orders of magnitude energy deficiency between the projected ratio (Newman and Okal, 1998).

The waves generated from a landslide event and an earthquake source are distinctly different. Earthquakes rupture along fault planes and can cause large waves that have very far reaching effects. The waves generated are strongly related to the magnitude of the seismic event figure 1.1 (Newman and Okal, 1998; DeLange and Moon, 2004), and are characterized by their long periods, (tens of minutes), and large wavelengths, (hundreds of kilometers); this is in contrast to wind waves which have wavelengths of up to 200m and periods of 0.5 to 30 seconds (see Synolakis (2003) who quotes Prager (2000)). Wind waves also have very weak energy attenuation since energy attenuation is inversely proportional to their period. In the near-field earthquake induced tsunamis also exhibit less radiation attenuation compared to that of landslide generated tsunamis since earthquake tsunamis stem from

a line source and landslides from a point source. This is obvious considering the rate at which energy concentration spreads from a point source compared to that of a line source. Another approach for understanding the differences in the waves generated from earthquakes and landslides is to examine the scale arguments comparing the vertical deformation of the sea floor with the linear deformation as presented by Synolakis et al. (2002). This type of scale argument is conducted by associating the extent of vertical deformation and horizontal dimension of both a landslide event and an earthquake event, and then proportionally associating that to the amplitude for the vertical length scale and wavelength and period with the horizontal length scale. By doing this it can be seen that earthquake induced tsunamis could have longer periods and wavelengths (therefore not as much attention) while landslide induced tsunamis have larger amplitudes. This in itself shows the great danger that landslide events can cause due to their large amplitudes in the near-field and ability to strike the coast quickly after initiation.

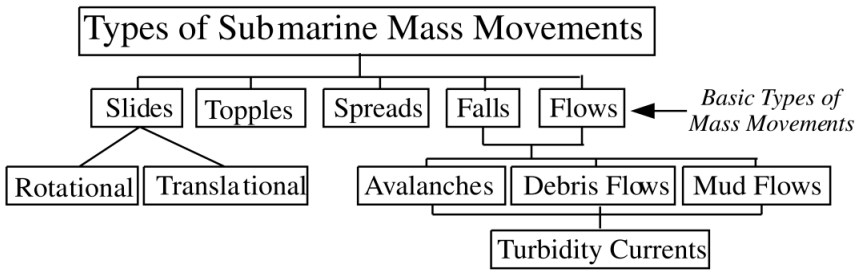

Fig. 1.2.: ISSMGE Technical Committee on Landslides (TC-11) classification of submarine mass movements adapted by Locat and Lee (2002).

Before going further it is important to note the ambiguity of terms when considering submarine landslides. The terms *submarine landslides*, *slumps*, or *mass movements* are used interchangeably by most authors and for the purpose of this discussion they will be used interchangeably here unless otherwise noted. Generally these events are characterized based on their material properties; see Hampton et al.

(1996); Locat and Lee (2002); Moscardelli and Wood (2008), and figure 1.2 is an example of the classification system used by the ISSMGE Technical Committee on Landslides adapted by Locat and Lee (2002).

Locat and Lee also modified a figure from Meunier (1993), figure 1.3(a) that shows the factor of safety, F, where F closer to zero indicates the higher potential of slope failure. They also list the possible elements that can initiate a submarine landslides. Figure 1.3(b) from Locat and Lee uses a schematic to describe the continuum of mass movements as a function of water and solid contents vs cohesiveness and granularity and then allocates whether the mixture will be best described by fluid mechanics, soil mechanics, rock mechanics, or hydraulics. This schematic does an exemplary job in describing the difficulty in modeling the continuum of these events.

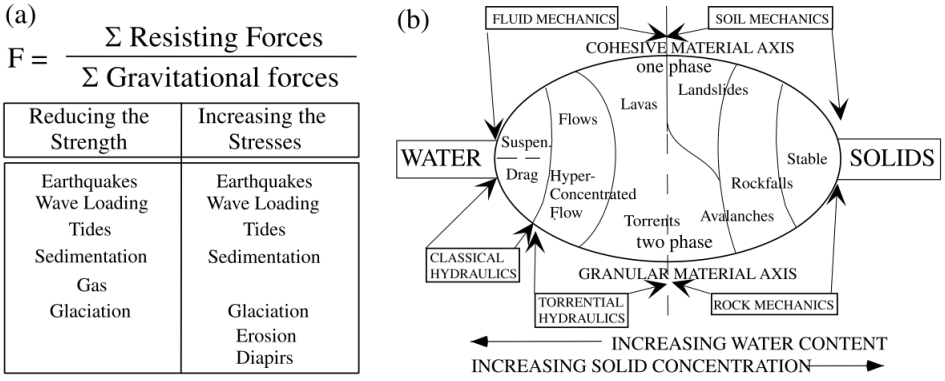

Fig. 1.3.: (a) Causes of submarine mass movements and factor of safety formula. (b) Schematic from Locat and Lee (2002) depicting the continuum of submarine mass movement events.

For the purposes of the rest of this discussion, unless otherwise noted, the slides will only be classified based on their location from sea level as in figure 1.4. This work will focus primarily on the farthest right example of the underwater slide or submarine event.

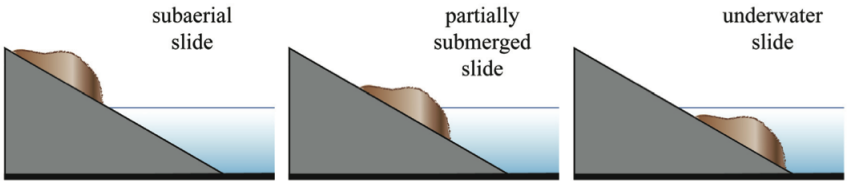

Fig. 1.4.: Pre-slide initial geometries for potential wave generation (Heller, 2008)

1.3 Research objectives

The general objective of this research is to determine if it is possible to quantify the time at which a submarine landslide is decoupled from the free surface and what effects viscosity, mass, and depth of submergence have on this separation time. In order to do this, a state-of-the-art hydrocode, iSALE, will be used to simulate wave generated from submarine landslides. This code is capable of modeling multiple materials, by varying over twenty different material parameters, in a geophysically realistic environment. It is the author's belief that this code will simulate soil fluid coupling accurately and therefore be appropriate for this task. This modeling effort will shed some light on the dynamics of this coupling event and lead to a better understanding of the time frame during which a slide is transferring energy to the free surface for wave generation. We are also aware that the material properties most likely change during slide evolution, and want to note that iSALE cannot account for this; however it is possible that the material properties are stable during the generation of the wave and this concern is unfounded. For this reason it is one of the goals of this present work to quantify the interval of time at which the slide is still coupled to the free surface and able to transfer energy. Another aspect of this work is to determine the influence that deformability has on runup. This modeling will also shed light on the significance that the shape of these bodies has on wave generation. Specific objectives are as follows:

1.3.1 Objectives

1. Are there any differences between runup heights generated from deformable submarine landslides and solid slides of the same geometry? How critical is the deformability of the slide in generating the wave height?

2. Are we able to accurately quantify the amount of time during which energy is transferred from the slide body to generate free surface deformation? What slide parameters effect this relationship?

3. What effects do the viscosity, mass, and depth of submergence have on the generated run up for fully deformable slides? To what degree do each of the parameters effect this value?

2. BACKGROUND

2.1 Analytical theories and numerical approaches

Compared to tsunamis generated by coseismic deformation little is known about the landslide generated waves. The waves generated by landslides pose a very vexing problem compared to earthquake induced waves since the rate at which energy is transferred in these events is relatively slow compared to that of seismic deformation events. In fact, during seismic events the energy transfer is fast enough compared to the speeds of shallow water waves that the initial conditions at the surface can be derived directly from the terminal deformation at the seafloor.

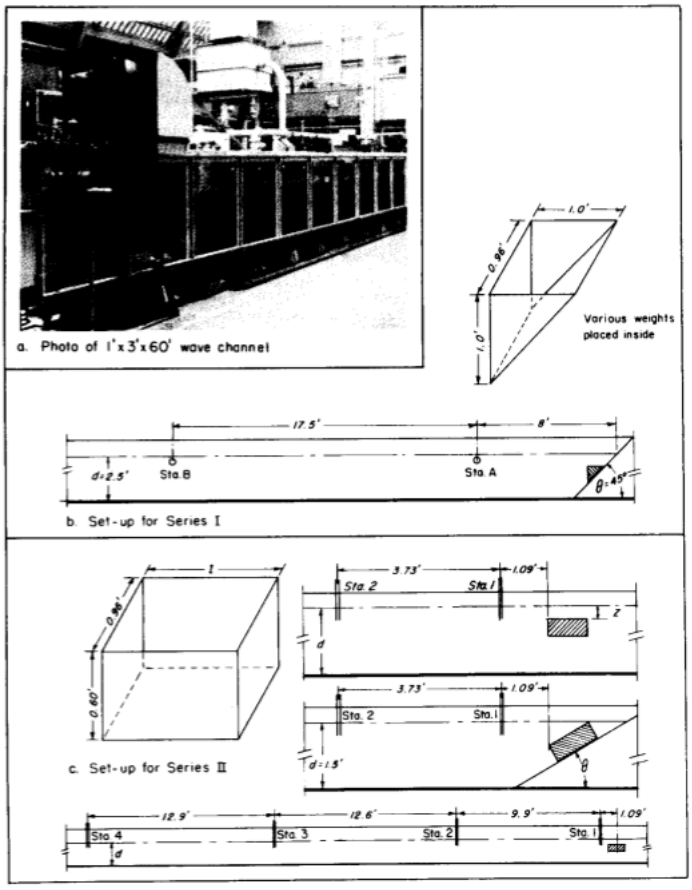

Fig. 2.1.: Experimental set up for Wiegel (1955).

Wiegel (1955) defined impulsively generated waves as waves generated by "the sudden movement of a submerged body for a short interval of time" which "may be considered representative of a submarine landslide." He initially conducted work on water waves generated by slumping gravel piles and sand impounded behind a vertical gate within a wavetank, however this work, was substituted for solid block landslides due to difficulties in engineering a release gate that did not generate waves (Sauer and Wiegel, 1946). Wiegel's experiments generated waves in a constant depth channel by releasing solid blocks of varying, shapes, densities, sizes, and initial depth of submergence, down a slope of varying inclination. He used resistance wave gauges to record the wave time history at given distances down the wave channel. Wiegel's experiments led to the conclusion that involved discovering that the leading wave in the far field wave train was always positive, depends on the water depth h and travels with the theoretical long wave velocity $v = \sqrt{gh}$, that the leading wave amplitude increased with inclination angle, block density, and shallower initial submergence, and lastly that the wave period was found to increase with increasing block length and decreased inclination angle. He also observed that immediately above the slide a trough occurred on the free surface and resulted in a rebound of similar magnitude. As for the energy, Weigel, calculated that there is a transfer of between 1-2% of the initial potential energy of the block was converted into wave energy and that this energy conversion increased with smaller submergence depths. It is also important to note that Wiegel's became the background for all future studies.

Supporting Wiegel's work, Stirem and Miloh (1975) did work on underwater landslides triggered by earthquakes off the coast of Israel. Their work highlighted the effect that these events had on sea level drawdown (10 meters) and on the duration (several hours). They posited that a signal solitary wave was generated for events of this nature and calculated the wave height based on the $\approx 1\%$ energy conversion. They highlight four different events to have occurred within the historical record off the coast of Israel.

Following the work done by both Wiegel and Striem and Miloh, Murty (1979) derived an equation for wave height using the energy released from a moving block sliding down an inclined plane from its initial position to its final position and then converted that energy into a solitary wave.

$$H = \frac{1}{D}[8(3)^{\frac{1}{2}}\mu l h(\gamma - 1)(D_o - D_s)]^{\frac{2}{3}} \tag{2.1}$$

In this equation H represents predicted wave height, D the reference depth far offshore, μ the energy transfer coefficient and γ the specific gravity of the slide material. All other variables in equation 2.1 are defined in figure 2.2. Equation 2.1 is the most commonly used estimation formula for the "height" of landslide generated solitary water waves, and works well in most cases when accurate parameters for the variables are known.

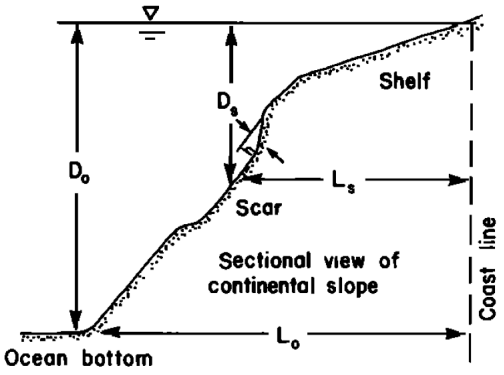

Fig. 2.2.: Murty (1979) landslide variables sketch.

Between 1975 and the 1990 very little work was done on the subject of landslide inducted tsunamis. One study to note, simply because it highlights the lack of researchers in this field during this time period, was done by McCulloch (1985). McCulloch, when estimating the landslide danger off the coast of southern California made an arithmetic error of two orders of magnitude, 0.14m vs. 14m. This error

drastically underestimated the danger off the California coast, and went undiscovered until Borrero (2002) identified and corrected the error 17 years later.

In the early 1990's, a two-dimensional finite difference solution algorithm of the Navier-Stokes equations to model wave generation from landslides was used by Heinrich (1992). This package, Nasa-Vof2D, was used to model waves generated by solid right triangular blocks sliding down an inclined plane. The fluid in this experiment was treated as incompressible, and the results compared favorably with laboratory experiments. For more information on these experiments see section 2.2-Laboratory modeling approaches.

More work on Nasa-Vof2D was conducted by Heinrich and peers, see Rzadkiewicz et al. (1997) and Mariotti and Heinrich (1999). Here they introduced a modified version of the code to simulate deformable submarine landslides. They assumed that the landslides would separate into two distinct layers: a dense flow near the slope slide interface, and a dispersive layer at the slide water interface that mixed with the ambient water via a diffusion model. The dense layer was modeled as a visco-plastic fluid and the dispersive layer as an ideal fluid. An interstitial pressure within the landslide and a sediment erosion-diffusion law at the soil-water interface was also introduced. This allowed for the permeability of the different "fluids" to be modeled and for a better simulation of sediment materials. The results compared well with laboratory experiments conducted.

Jiang and LeBlond (1992) proposed a model for wave generation where the landslide was treated as a laminar incompressible viscous fluid and employed a finite difference method to solve the resulting differential equations (2 layer 2+1 dimensional shallow water equations). Their experiments released a parabolic shaped mass sliding, and deforming due to gravity, down an inclined plane. Their goal with the experiments was to model and analyze the coupling between the landslide and the water. To do this they used three scenarios, in the first they only modeled the landslide behavior under a fixed surface, in the second they allowed the motion of the

slide to effect the free surface, and thirdly they allowed the pressure gradients on the free surface to also effect the process. They found that the wave amplitudes generated depended greatly on the slide density, initial submergence, landslide volume, and viscosity of the slide material. It was also argued that the density and initial submergence of the slide were the two dominating factors in determining the interaction between the slide and the waves that were generated and that the transfer of energy was not constant and decreased after initiation to around to only 2% to 4% after the slide propagated into deeper water. They proposed $\mu = 15\%$ as a total energy transfer rate.Jiang and LeBlond (1993) incorporated a Bingham plastic constitutive relation into their model to simulate rigidity under the influence of motion. Interestingly, LeBlond and Jones (1995) used these results to discount the ability of submarine landslides to generate tsunamis.

Watts (1997, 1998) studied waves generated by submarine landslides, while at the California Institute of Technology working under Fred Raichlen. He conducted laboratory experiments and proposed equations for generated surface waves that have become the most common for estimating landslide waves at geophysical scales (Borrero et al., 2001; Tappin et al., 2001; Synolakis et al., 2002; Okal et al., 2002; Okal and Synolakis, 2004).

Watts (1997), validating Pelinovsky and Poplavsky (1996) work, derived a force balance equation on a submerged solid block sliding along a plane inclined at angle θ.

$$(m_b + C_m m_o)\frac{d^2 s}{dt^2} \approx (m_b - m_o)g(\sin\theta - C_n \cos\theta) - \frac{1}{2} C_d \rho_o \omega l \cos\theta \sin\theta \left(\frac{ds}{dt}\right)^2 \quad (2.2)$$

In equation 2.2 s is the instantaneous position of the center of mass, m_b is the mass of the sliding block, m_o is the mass of the displaced fluid, ρ_o is the density of the fluid, ω is the width of the block, l is the length of the block along the incline, and C_m, C_n, C_d are the coefficients of added mass, Coulombic friction, and fluid dynamic

drag, respectively (Synolakis, 2003). Pelinovsky and Poplavsky (1996) argue that the terminal velocity is reached when $\frac{d^2S}{dt^2} = 0$ and they derived the terminal velocity and initial acceleration as:

$$u_t = \sqrt{\left(\frac{2gl}{C_d}\right)(\gamma - 1)(\sin\theta - C_n \cos\theta)} \tag{2.3}$$

$$a_o = \frac{\gamma - 1}{\gamma + 1} g \sin\theta \tag{2.4}$$

Watts (1998) and Borrero (2002) simplified this expression and solved for a semielliptical slide body. They set $C_m = 1$, $C_n = 0$, and used an experimentally derived term for $C_d \sin\theta \cos\theta$ and simplify:

$$u_t = \sqrt{0.5gl \cos\theta \pi(\gamma - 1)(\sin\theta)} \tag{2.5}$$

Watts and Borrero (2001) further extend pervious work and with an empirical expression which describes a characteristic two-dimensional tsunami amplitude of a sliding ellipse down an inclined plane; equation 2.6.

$$\eta_{2d} \approx s_o \left(0.05096 \sin\theta - 0.0328 \sin^{2.25}\theta\right)\left(\frac{T}{b}\right)\left(\frac{b}{d}\right)^{1.25} \tag{2.6}$$

In equation 2.6, η_{2d} represents the two dimensional amplitude, s_o the characteristic "run" of the slide defined as $\frac{u_t^2}{a_o}$, T the thickness of the ellipse, d the depth of the top of the ellipse, and b the length of the ellipse measured along the slope. For rotational slides, see equation 2.7, where the radius of curvature R is also needed along with a rotational parameter $\delta\phi$.

$$\eta_{2d} \approx s_o \delta\phi^{0.39} \left(0.1308 \sin^{0.22}\theta\right)\left(\frac{T}{b}\right)\left(\frac{b}{d}\right)^{1.25}\left(\frac{b}{R}\right)^{0.63} \tag{2.7}$$

It is argued by Watts and Borrero, that this empirical formula is valid for $T < 9.2L$, $L < R < 2L$, $d > 0.06L$, $\theta < 30$, and $\Delta\phi < 0.53$. It is important to remember

that these formulas represent a characteristic tsunami amplitude and not a particular wave height at any point along the free surface. The equations were derived from curve fits of numerical and experiments results.

Borrero (2002) used Watt's work on characteristic tsunami amplitude to derive expressions for the location of the maximum depression X_{min} and the distance from the crest of the elevation wave to the trough of the depression wave ΔX. He also derived expressions for the height of the maximum elevation wave Z_{max}, and minimum depression wave Z_{min}. With these expressions it is possible to completely describe a particular event's wave shape.

$$X_{min} = 0.95\left(X_s + 0.4338 s_o \cos\theta\right) \tag{2.8}$$

$$\Delta X = 0.5 t_o \sqrt{gd} = 0.5\lambda \tag{2.9}$$

$$Z_{min} = 2.1\eta_{2d} \tag{2.10}$$

$$Z_{max} = 0.64\eta_{2d}\left(0.8 + \frac{0.2d}{b\sin\theta}\right) \tag{2.11}$$

Bohannon and Gardner (2004) altered Murty's formula and asserted that the energy term $\mu\rho g\omega\lambda a^2$ is contained within one sinusoidal wave of height a and wavelength $\lambda = 2t_o\sqrt{gd}$. They rederived the formula considering a mass dropping from a distance of Δz (equation 2.12).

$$H = \sqrt{\mu(\gamma - 1)LT\frac{\Delta z}{\lambda}} \tag{2.12}$$

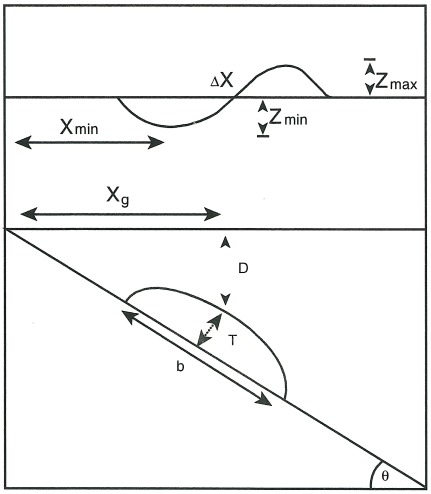

Fig. 2.3.: Landslide generated waves variables definition sketch (Synolakis, 2003).

Synolakis (2003) argues that Bohannon and Gardner (2004) equation 2.12, requires both a specification of Δz the drop of the slide, and a transfer coefficient constantμ that will undoubtedly not be constant as it changes with depth as per Jiang and LeBlond (1992). Working along with his Ph.D. student at the time Burak Uslu, Synolakis used analytical results and assumed that the initial wave generated within a horizontal motion was no longer then half of the slide's length. They proposed that the energy transferred is similar to that of a wave maker for the first ten seconds of motion, and that the initial wave is generated within a time using a_o:

$$t_o = \left(\left(\frac{1}{4} \right)^{\frac{1}{3}} \sqrt{\frac{d}{g}} \left(\frac{g}{a_o} \right)^{\frac{1}{3}} \right) \tag{2.13}$$

$$a_o = \frac{\gamma - 1}{\gamma + 1} g \sin\theta \tag{2.14}$$

They then calculated the net energy of a isosceles N-wave with height H see equation 2.15.

$$\epsilon = \frac{2}{3}\sqrt{3}\pi\rho g w \left(dH\right)^{\frac{3}{2}} = \frac{\rho g L T w \Delta z}{2} \tag{2.15}$$

Δz was set to $\Delta z = (1/2)a_o t_o^2$. In this analysis the heights of the maximum and minimum crest of their waves were considered equal. Their final result was to get a new formula for wave height that does not depend on Δz or any empirical factors (Synolakis, 2003).

$$H = 0.139 \left(\frac{L^2 T^2}{d}\right)^{\frac{1}{3}} \left(\frac{a_o}{g}\right)^{\frac{2}{9}} \tag{2.16}$$

A series of numerical three dimensional landslide generated wave experiments were conducted by Grilli et al. (2002) using a three dimensional potential flow solver of the Navier Stokes equations employing a Boundary Element Method (BEM). Their results estimate the effect of the generated wave as the width of the landslide is varied.

Landslide motion is modeled by Ward (2001) as the movement of solid blocks allowing each moving block to interact with the water column and generate waves. This method allows for the creation of complex geometries by combining blocks with prescribed velocities. Ward and Day (2001, 2003) applied this method to both the Cumbre Vieja Volcano and Ritter Island Volcano collapse.

Lynett and Liu (2002) used a depth integrated formulation to model rigid body slides and validated their algorithm using the experiments of Hammack (1973). Liu et al. (2003) reached conclusions regarding the effects that the slope, slide length, and thickness have on generated waves for a rigid Gaussian shaped slide. Their experiments where run with their proposed exact solution of a forced linear wave equation.

Capone et al. (2010) used the method known as smooth particle hydrodynamics to model the 2D motion of the Rzadkiewicz et al. (1997) slide experiments.

2.2 Laboratory modeling approaches

In Sauer and Wiegel (1946), performed a series of experiments in an attempt to generate waves with granular materials. Their experiments consisted of placing a steep pile of gravel on top of a piece of sheet metal at a 45 degree slope at one end of a 60 ft long by 3ft high by 1 ft wide channel. They then attempted to pull the piece of sheet metal out from under the slide in order to disrupt equilibrium and cause slope failure. However when the sheet metal was pulled out only a slump of the material occurred and no waves were generated. Their next attempt was to pile sand behind a vertical grate and then remove the grate to cause slope failure. This resulted in two sets of waves being generated, one from the slope failure, and one of the same order of magnitude from the grate being removed. Luckily, Weigel's instincts lead him to conduct another series of experiments, which were discussed in the previous section, to set the stage for the analytical and numerical approaches discussed. His definition of a submarine landslide, introduction of a wedge model, proof of the potential for landslides to generate waves, and discussion of variants in the system established a strong foundation for future work.

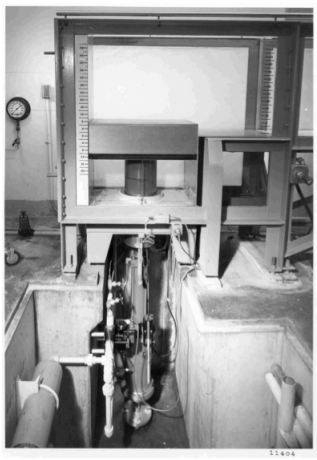

Fig. 2.4.: Photograph of Hammack's wave tank and piston generator (Hammack, 1973).

Hammack carried on this work in the 1970's as a PhD student under Fred Raichlen by generating tsunamis with the vertical motion of a piston. In his experiments the piston was initially flush with the bottom of the tank and then hydraulically controlled, see Figure 2.4. Even though these experiments are more characteristic of an earthquake generated tsunami, they made a significant discovery for understanding landslide generated events. Hammack (1973) discovered that if the piston was moved slower than the the wave propagation out of the generated region, then the wave heights that were generated out of the region were independent of the aspect ratio of the generated region, and that the wave heights were dependent on the inverse power of the time of wave generation. This concept is especially important when considering a landslide event, i.e. an event that only transfers a variable amount of energy during the variable movement period of the slide. This early work sheds light on the subject of this present work, and emphasized the need to quantify the amount of time during which slides transfer energy to wave generation.

In order to validate his numerical model, Heinrich (1992) conducted one underwater landslide experiment with a weighted block that slid on rollers down 45° inclined plane into a channel with constant depth of 1m. This block was in the shape of a right triangle of 0.5m long, and had a mass of 140kg and a density of $2040 kg/m^3$. The block was placed on the incline 1cm below the surface of the water making it submarine. Figure 2.5 shows a comparison between Heinrich's numerical code and experimental data for a submarine landslide event. Heninrich later revisited these experiments with Rzadkiewicz et al. (1997) in order to validate later numerical models. This study simulated right triangular solid masses and granular sand and gravel sliding down inclined slopes of varying degrees. Their goal in these experiments was to measure the landslide velocities.

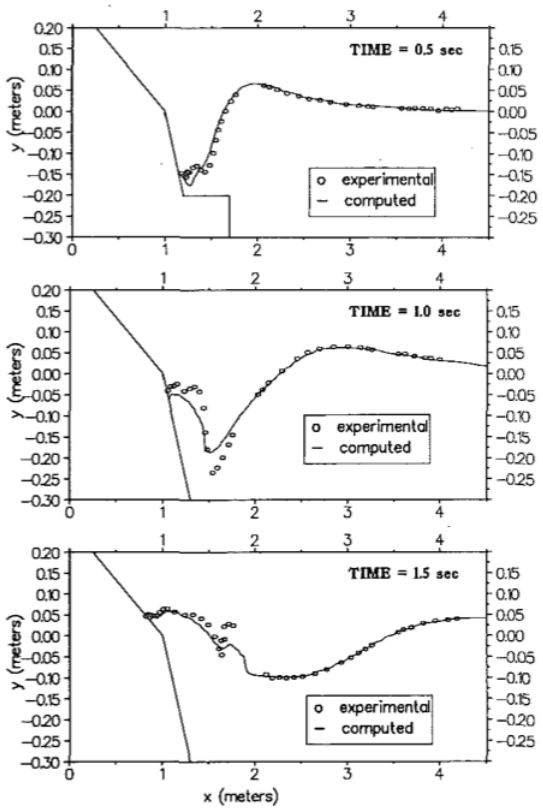

Fig. 2.5.: Comparison between Heinrich's numerical and experimental wave profiles for a submarine landslide placed 1cm below still water level. Times at $t = 0.5s$, $t = 1.0s$, $t = 1.5sec$

Watts (1997, 1998) conducted both granular and rigid body experiments using a 36.6m long, 0.38m wide, and 0.61m deep flume at The California Institute of Technology. His experiments consisted of solid and granular slides, sliding down a 45° slope only under the influence of gravity. Figure 2.6 shows the schematic drawing of the apparatus used.

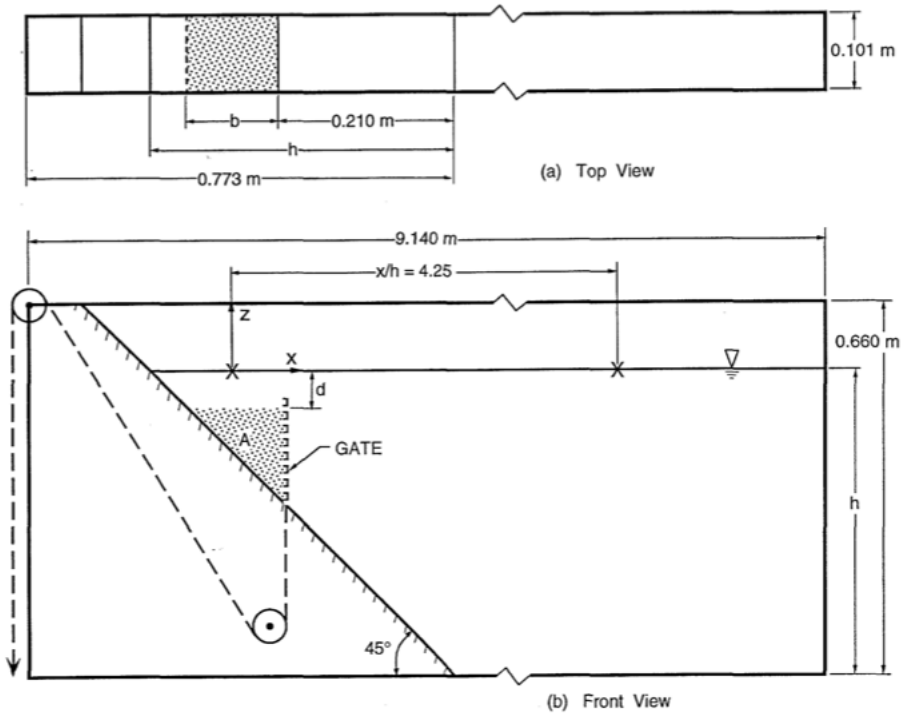

Fig. 2.6.: Watt's schematic drawing of the experimental apparatus used in his submarine landslide study with a) top view b)side view (Watts, 1997)

He varied the weight of the blocks he used and measured the accelerations of these blocks down the incline. He noticed that the block accelerated rapidly to a terminal velocity under the influence of gravity. Watts (1997) also measured the water level time histories for his experiments. This can be seen for a number of masses in figure 2.7. In figure 2.7 a) the complex nature of the the dynamics of free surface directly under the slide body (between 0-1s) can be observed. The present author is defining this area as the landslide induced cavity and defines the decoupling or separation time as τ here occurring sometime within the described window.

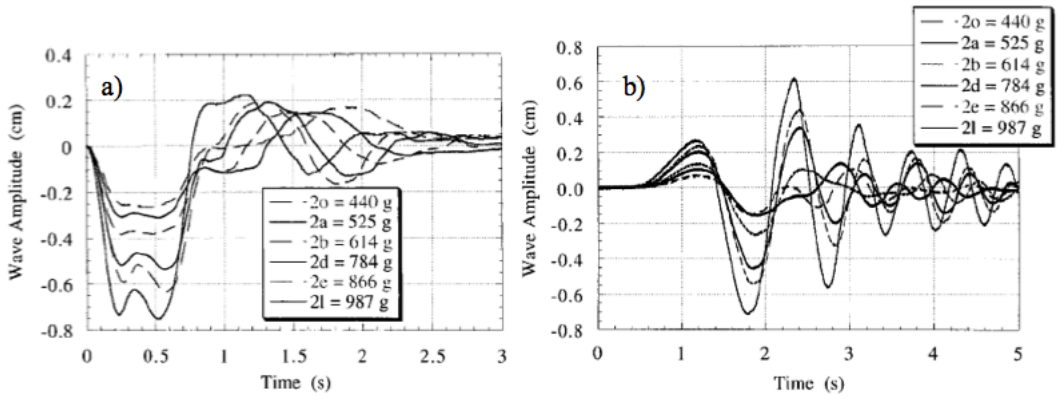

Fig. 2.7.: Water level time histories from Watts (1997) for a number of different masses. a) Shows near field water level history b) shows far field water level history.

In an effort to understand generation, propagation, and run-up of waves generated from submarine landslides,Liu et al. (2005) conducted a series of experiments in a wave tank at the Oregon State University, Corvallis Oregon in a 104m-long, 3.7m wide, and 4.6m-deep wave channel. A plane slope with a inclination of 1:2 (26.27°) was located at one end of the tank. Water filled the tank to ≈2.44m. Two wedge shaped solids and one hemispheric solid block were used to simulate landslides. Figure 2.8 shows a sketch with the variables in the experiments they labeled as series A. The wedge had the following dimensions, a: 45.72cm, b: 91.44cm, and width: 65.25cm. For series B the slide was rotated so that b becomes the front face.

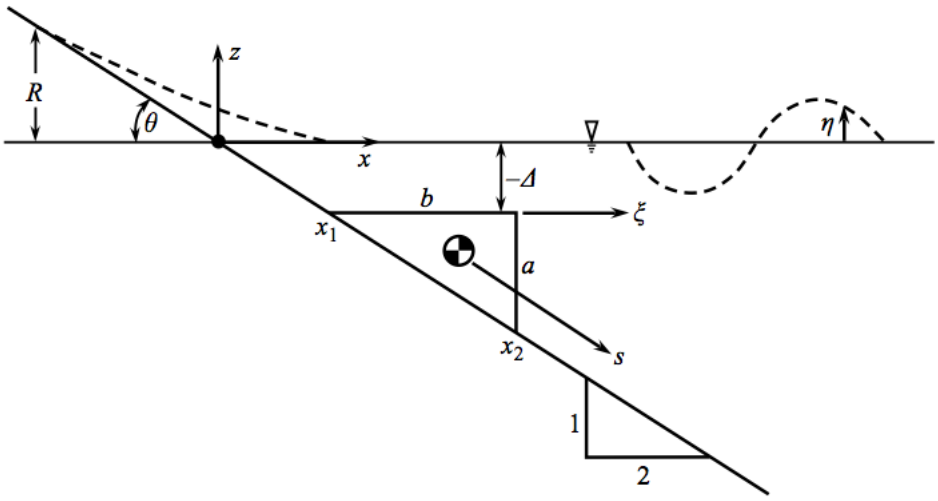

Fig. 2.8.: Definition sketch for Liu et al. (2005) experiments.

Table 2.1 gives a list of the masses used for the respective wedges and the hemisphere. Figure 2.9 shows an example of the slide in motion during one of the experiments. Notice the positive leading wave in front of the slide and the depression following in the wake of the slide.

Table 2.1: Masses used in experiments conducted by Liu et al. (2005).

Wedge A	Wedge B	Hemisphere
190.96 kg	273.44 kg	394.73 kg
273.44 kg	355.92 kg	354.44 kg
355.92 kg	437.57 kg	637.08 kg
436.75 kg		
475.52 kg		

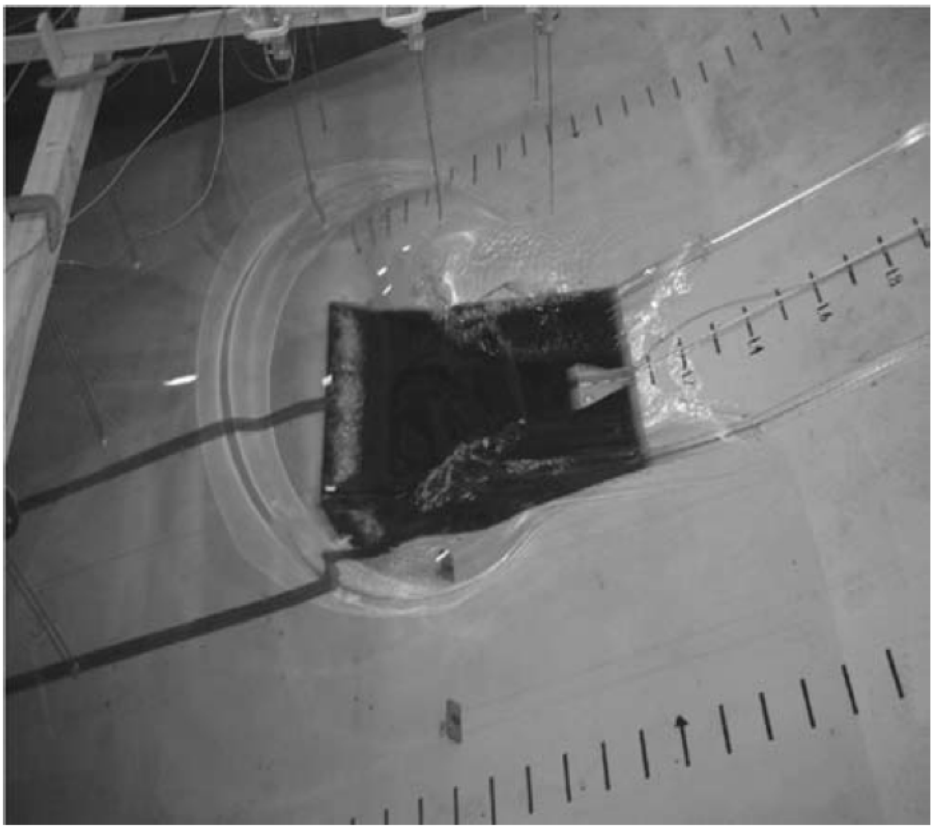

Fig. 2.9.: Photograph from Liu et al. (2005) large scale laboratory experiments. Notice the positive leading wave in front of the slide and the depression following from a series b experiment.

By varying the weights of the blocks in these experiments, they were able to vary the initial acceleration. It was noticed that as the depth of submergence Δ became larger than one block height, wave generation became increasing inefficient. This can be seen in Figure 2.10 which is a chart of run-up R (nondimensionalized by slide length b) versus depth of submergence Δ (nondimensionalized by slide length b) times γ. It can be seen in this figure that with decreasing depth of submergence and increasing mass, run-up increases and that for different slide shapes the overall magnitude of wave generation is different. Therefore they concluded that there is a dependence of landslide shape on water wave generation.

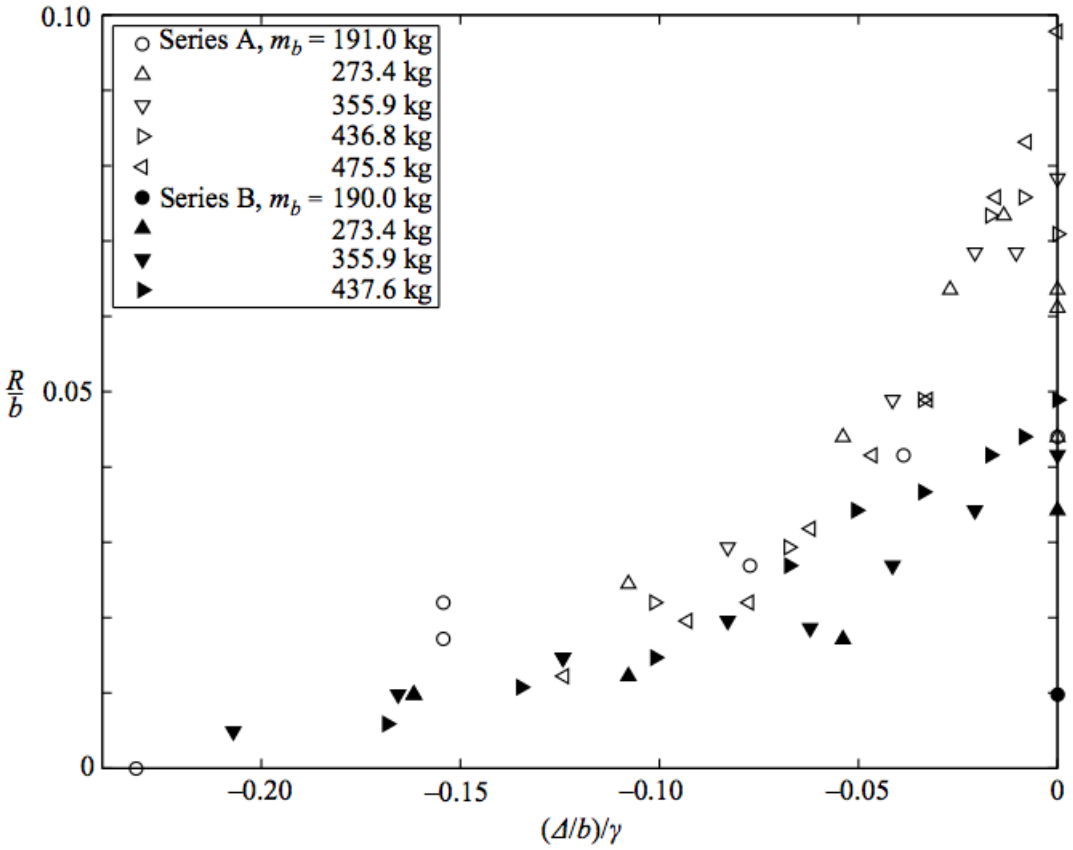

Fig. 2.10.: Liu et al. (2005) graph of nondimensionalized run-up versus nondimensionalized depth of submergence.

These experiments became the benchmark for the National Science Foundation Catalina workshop to validate runup models. This current work is modeled after this series of experiments, which will be discussed in Section 3.0.

Other laboratory experiments to note were conducted by Grilli and Watts (2005). Their numerical simulations involved a two dimensional non-linear potential flow consisting of a semi-elliptical rigid slide, sliding down a planar slope. They compared their numerical results to the laboratory results and concluded that the experiment was accurate within the accuracy of the experimental measurability. They also wrote that "for rigid slides of Gaussian shape, both near and far field tsunami amplitudes increase if shape of spreading decreases." This "shape change" is assumed to refer

to Gaussian or elliptic shapes with different aspect ratios, continuously deforming slides, but not following any particular constitutive relationships. Walder et al. (2003) also model rigid slides and develop empirical correlations between the leading wave height, the volume of the slide, and a dimensionless time.

Herman Fritz conducted a series of experiments at the Swiss Federal Institute of Technology which are considered the current benchmarks for subaerial deformable slides(Fritz, 2002, 2000; Fritz et al., 2003a,b, 2004). In these experiments granular subaerial landslide-generated tsunami waves were investigated in a rectangular prismatic water wave channel 11m long, 0.5 m wide, and 1m deep, with still water level at h=0.30m, 0.45m, and 0.675m. The deformation of these bodies was imaged with lasers. He concluded that for the wave generation of subaerial slides the relevant parameters were: slide impact velocity, still water depth, and slide thickness. The physical model results were then used to reconstruct the impulsive wave that struck Lituya Bay Alaska in 1958 (Miller, 1960) and produced runup in excess of 520m along the steep fjord walls of Lituya Bay. A cross section of area was rebuilt in the laboratory at a small scale (1:675) and the measured run-up matched the forest destruction (Fritz et al., 2001).

2.3 Evaluation of current approaches

Figure 2.11 shows estimates of the leading wave height as computed using four different wave formula, including variations of Synolakis (2003); Watts (1997); Pelinovsky and Poplavsky (1996); Bohannon and Gardner (2004) for a total of ten calculations per each set of slide parameters. Notice the large range of values for any nondimensional slide (abscissa), for figure 2.11A) wave amplitude is nondimensionalized by slide width b on the ordinate and $\tan(\beta)$ represents the slope inclination which is multiplied by slide height h and length L for figure 2.11B) the ordinate is the same as in A) but the abscissa is specific gravity times the distance from the free surface to the top of the slide D_s divided by the slide length L. This range of up

to 8 orders of magnitude from some slides presents that it is clear from the present state-of-the-art formulations more progress is needs to be made for the validation of these equations with numerical and laboratory experiments. This large range of estimated wave heights is one of the major motivations for this current work.

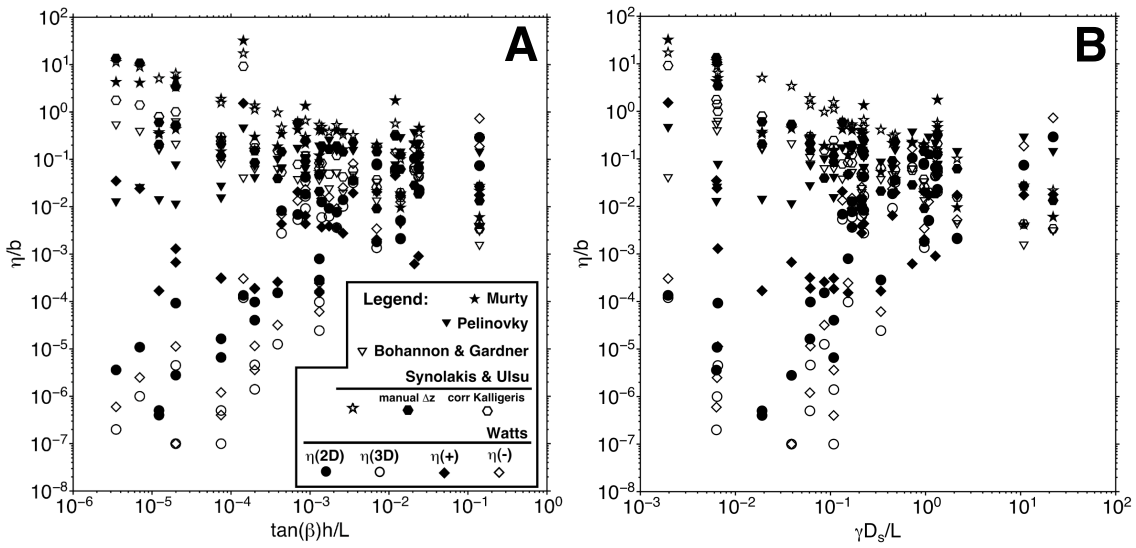

Fig. 2.11.: Scaled initial wave height predictions (ordinate) for a given landslide and two different slide geometry scalings (abscissas); different symbols correspond to various empirical formula Weiss et al. (2011).

2.4 Hydrocode modeling

The computational model used in this current study to model submarine landslides is called iSALE, which is an acronym for impact Simplified Arbitrary Lagrangian Eulerian hydrocode(Amsden et al., 1980; Wunnemann et al., 2006). Hydrocodes are numerical programs that simulate highly dynamic events, such as the flow of fluids and the deformations of bodies occurring at speeds at or near hypervelocity (Anderson, 1987; Johnson and Anderson, 1987). This is the the velocity

in a given reference frame for the speed of sound. The two codes to be discussed below and have both been used in modeling submarine landslide induced tsunamis and were developed at Los Alamos National Laboratory (LANL).

To the author's knowledge there have been two different hydrocodes used to model impulsively generated wave events. The better known of the two is a hydrocode SAGE and will be discussed here only briefly. This program is defined as "a multi-material adaptive-grid Eulerian code" (Mader and Gittings, 2002). It solves the full set of compressible Navier-Stokes equations, and employs a continuous adaptive mesh refinement algorithm (CAMR) to refine the grid, depending on the gradients in the physical properties, at every iteration of the program. This program allows for a number of materials and can allow for any cell to contain all materials defined in the problem even if they are associated with different equations of state. This code has been used for both the modeling of landslide events Mader and Gittings (2002); Gisler and Weaver (2006) and impact events Gisler et al. (2003, 2004).

iSALE was developed first as SALE, Simplified Arbitrary Lagrangian Eulerian, by Amsden et al. (1980). The codes initial uses include modeling the effects of nuclear explosions and testing the effect of high velocity air flows over fighter jet wings. Since the 1990's many contributors have improved and added versatility to the code. These contributors include Melosh who added a elasto-plastic constitutive model (Melosh et al., 1992), a Grady-Kipp fragmentation algorithm (Melosh, 1984, 1987) and a Tillotson equation of state (Tillotson, 1962). Ivanov et al. (1997) further modified iSALE by incorporating a free-surface and material interface tracking in the Eulerian mode, incorporated damage accumulation and strain weakening into the constitutive model, and added a semi-analytical equation of state ANEOS (Thompson and Lauson, 1972). Wünnemann added improvements that allowed the incorporation of a third target material and the ϵ-α porous-compaction model (Wünnemann and Ivanov, 2003; Wünnemann and Morgan, 2005; Wunnemann et al., 2006). Collins improved the constitutive model of iSALE and added improvements to the interface

reconstruction method to reduce the numerical diffusion of low volume materials, and improvements to the porous compaction model for simulating impacts in high porosity target materials (Collins et al., 2004).

One of the benefits of iSALE is its geophysical realistic constitutive model employed for the various materials that can be incorporated in the simulations. In fact twenty different material parameters can be specified in iSALE including:

- the Poisson ratio
- the strength at zero pressure (intact; MPa)
- the strength at infinite pressure (intact; MPa)
- the strength at zero pressure (damaged; MPa)
- the friction coefficient
- the volumetric strain at the elastic limit
- the brittle-ductile transition pressure
- the internal friction coefficient of the intact material
- the brittle-plastic transition pressure
- the melt temperature (degrees Kelvin)
- the specific heat capacity (J/Kg/Kelvin)
- the tensile strength (MPa)
- the thermal softening parameter
- the Simon parameters for Melt T. vs P.
- the initial distension

- the exponential compaction rate
- the initial porosity
- the volumetric strain when fully compacted
- the volumetric strain at transition

It is not currently clear which of the parameters are going to be critical in order to better understand water wave generation from submarine landslides, and since it will not be feasible to conduct the number of runs necessary to test each one of these, we will began with a small set of parameters that we have selected and try to quantify their effect.

2.4.1 Impact modeling

The initial use of iSALE was to model meteor or asteroid impacts on the surface of a planet or planetesimal. Therefore extensive work has been conducted in this area (Melosh et al., 1992; Ivanov and Deutsch, 1999; Ivanov and Artemieva, 2002; Wünnemann and Ivanov, 2003; Collins et al., 2004; Wünnemann and Morgan, 2005; Ivanov, 2005). iSALE (and SAGE, to a lesser extent see (Gisler et al., 2003)), have also been used to study the waves generated from bolide impacts into the ocean (Wünnemann and Lange, 2002; Weiss et al., 2006; Weiss and Wünnemann, 2007).

2.4.2 Landslide modeling

Mader and Gittings (2002), and Gisler and Weaver (2006) have both employed the hydrocode SAGE to model landslide induced tsunamis hazards. Mader and Gittings simulated the Lituya Bay Alaska event and calculated a maximum wave height of ≈580m compared to the measured ≈520m. Their work did not include any wave gauge data for comparison with Fritz et al. (2001), therefore it is difficult to understand the sensitivity of their program and whether or not it could be

used a parametrized based study. Gisler and Weaver (2006) simulated the proposed La Palma landslide threat, Figure 2.12, as posed by (Ward and Day, 2001). They concluded that even the largest estimates of the threat they could generate is "considerably smaller" then the worrisome values given by Ward and Day.

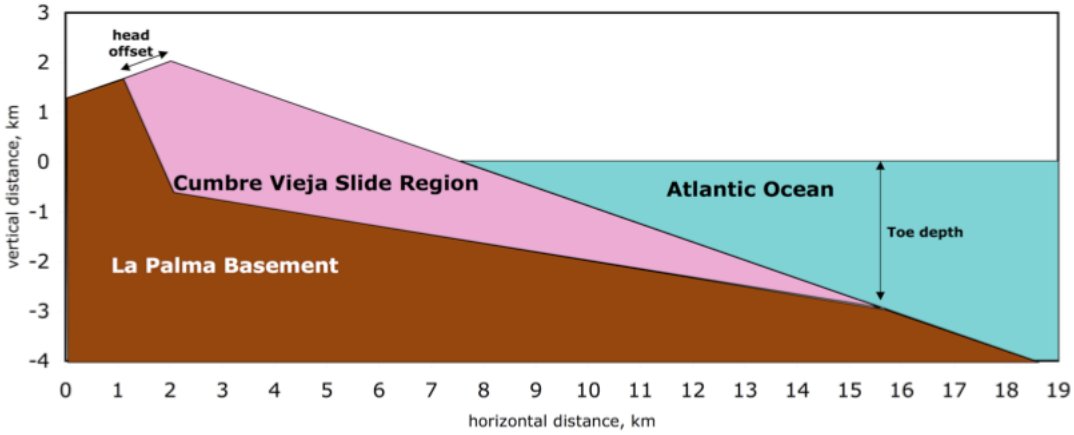

Fig. 2.12.: Gisler and Weaver (2006) schemtaic set up of the LaPalma landslide for two dimensional model runs conducted by SAGE.

Results of work with iSALE on landslide modeling was presented were first presented by Weiss et al. (2009), to the EGU General Assembly as a research abstract. This work presented the comparison of wave gauge data with Fritz et al. (2001) benchmark data with impressive results. This initial work was the catalyst for this present study.

2.4.3 iSALE validation

An 8.3 magnitude earthquake struck the coast of Alaska and was reported to cause the bay area to shake for up to 4 minutes. After this earthquake $\approx 30 \times 10^6 m^3$ of rock turned into a sub aerial landslide and slid down the wall of the Gilbert Inlet

at the head of the Lituya Bay causing a runup on the opposite slope of 524m. This currently the largest runup recorded in history.

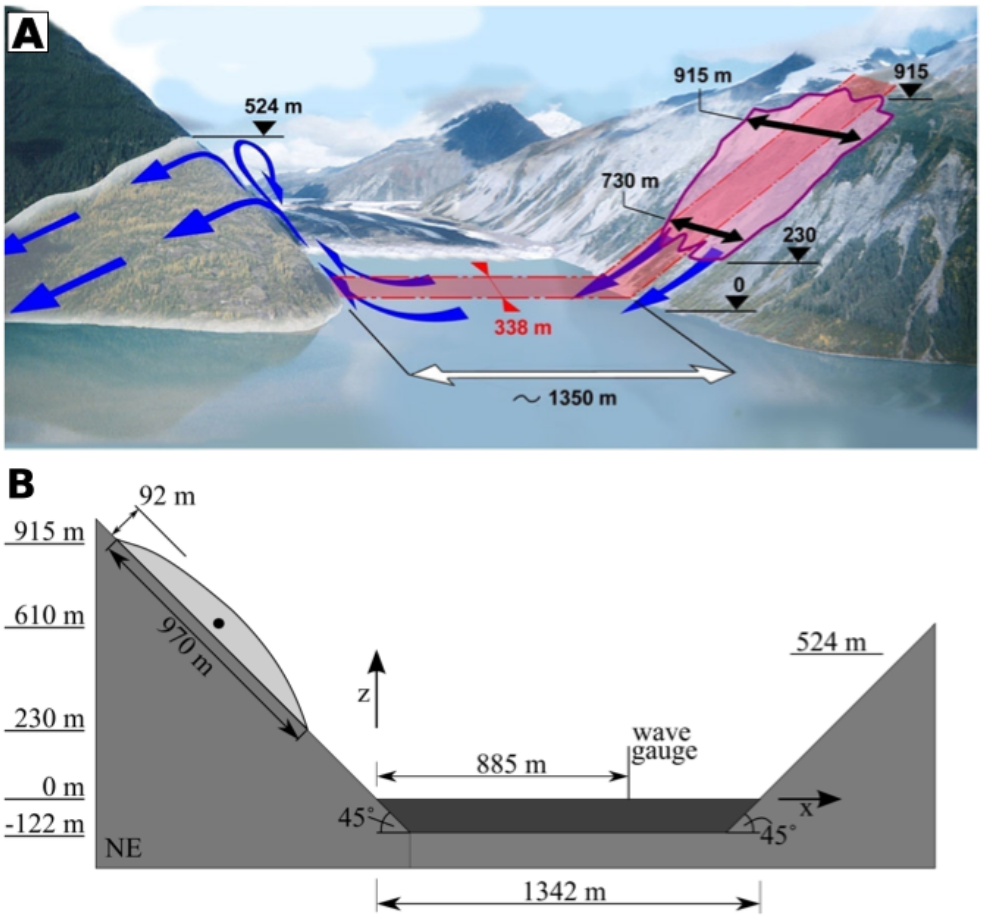

Fig. 2.13.: A - Illustration of the Gilbert Inlet in Lituya Bay showing the rockslide, per Fritz et al. (2001). B - Simplified geometry as used in the laboratory experiments and the computions Weiss et al. (2009).

The iSALE validation experiments were conducted under the same parameters as the Fritz et al. (2001). Figure 2.13 a) shows Gilbert Inlet in Lituya Bay Alaska, and b) shows the simplified geometry that Fritz used. The geometry was created at a 1:675 scale, but the measurements given are in their unscaled values. The slopes at the banks of the fjord were placed 45° from the horizontal, the banks 1342m

apart, with 122m of water in the bottom of the bay. The slide was made to be 970m long, 92m high with the center of mass was placed 610m high on the slope. A wave gauge was placed at 885m from the side marked NE in figure b, this was used to monitor the wave height at all times during the experiment. This same geometry was constructed by Weiss et al. (2006) with iSALE, see Figure 2.14 a. One difference between the Fritz et al. (2001) and the Weiss et al. (2009) experiments was the shape of the slide, however deformation occurred during the Fritz laboratory experiments so this difference should not greatly effect the outcome. Another difference is that Weiss did not build the numerical model with the 1:675 scale and instead used the actual length scales in the experiment. Figure 2.14a) shows initial setup used by Weiss and b) the slide deforming slightly before impact in the water. In c)($19s$) the first crest in g) is being formed, which occurs at $\approx 19s$, in d) ($21.5s$) a steep crest can be observed which precedes wave breaking and run-up onto the far slope. In graphic e) ($53s$) the direction of movement has changed corresponds to the second crest in the time series. It can been seen in the time series g) that Weiss's modeling with iSALE, in red, corresponds quite well to the Fritz et al. (2001) measurements in the dashed line for the first 60 seconds.

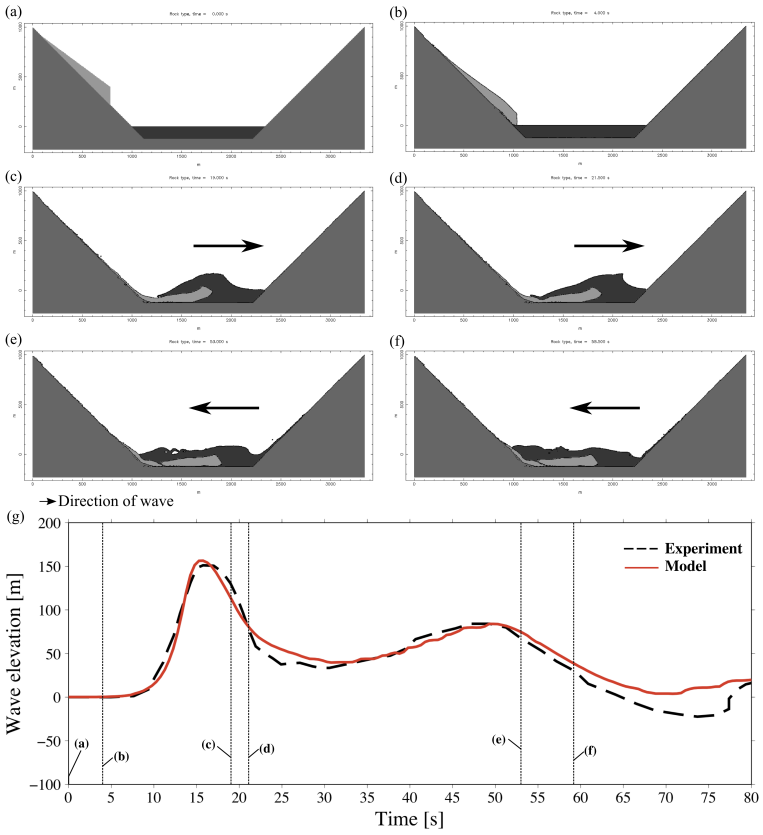

Fig. 2.14.: (a-f) Snapshots illustrating the water motion associated with the maxima in the time series. (e) Comparison between the experimental data from Fritz et al. (2001) and model results computed with the iSALE model Weiss et al. (2009).

With the quality of the fit we received between iSALE and Fritz's experiments, it is accepted that this will be an excellent tool to use in modeling this complex event under realistic geophysical conditions.

3. NUMERICAL EXPERIMENTS

3.1 Grids and geometries

iSALE is used for the numerical simulations conducted in this work. The analysis of this data is conducted using iSALE's post processing algorithm iSALEPlot and customized scripts written in Python, a versatile programming and scripting language.

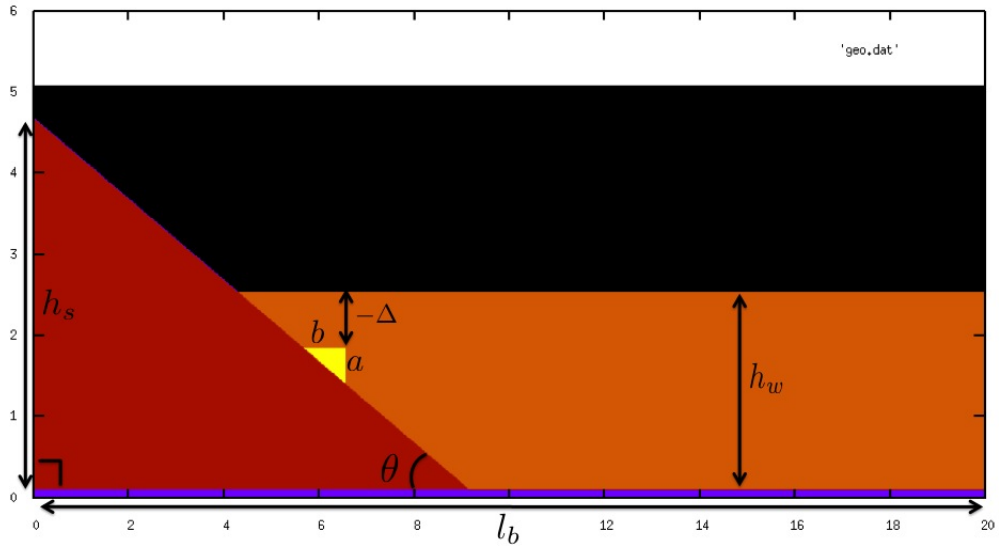

Fig. 3.1.: iSALE input file with respective variables labeled.

The geometric set up for the models was based on the experiments conducted by Liu et al. (2005). An example of the Fortran generated input file used in this work for iSALE can be seen in figure 3.1. In this image the slope is shown in red, the slide in yellow, and the water in orange. This figure has also been labeled with the respective variables: h_s for slope height, θ for slope angle, h_w for water depth, $-\Delta$ for depth of submergence, l_b base length, and a and b for the respective sides of the

slide body. The variable convention is based on the work done by Liu et al. and can be found in figure 2.8.

Table 3.1 lists the particular variables used in the numerical experiments. The values were derived from the dimensions of the wave tank and experimental set up used during the laboratory experiments of Liu et al.. In the numerical experiments the domain was shortened from 20 m to 16 m in order to shorten the computation time and because the area of interest for the current objectives lie in the near shore environment. The grid size used was 0.02 m and was determined also based on the computational expense and the necessity of a small grid size due to the overall scale of the experiment.

Table 3.1: Table of variables used in numerical experiments.

θ	26.56°
h_s	4.6m
l_b	16.0m
h_w	2.44m
a	0.4572m
b	0.9144m
dx	0.02m

3.2 Initial conditions

Two parameter variables are changed for the purposes of this current work, m (mass) and $-\Delta$ (depth of submergence). Five different masses were selected for these numerical experiments, these are the same five masses used in the series A experiments of Liu et al. (2005). These particular masses were chosen in order to compare the results of the numerical experiments with the results plotted in

figure 2.10. In this figure it can be seen that this series produced the largest runup therefore the slides in this series transferred the most energy into the water column. They also bound the entire range of masses in used in both the series A and B experiments conducted by Liu et al.. Table 3.2 gives a list of these masses.

Table 3.2: Table of masses used in numerical simulations.

Wedge A
190.96 kg
273.44 kg
355.92 kg
436.75 kg
475.52 kg

The masses were applied to the two dimensional problem in terms of their densities. This was calculated based on the masses and cross sectional area of the slides from the Liu et al. experiments.

The second parameter that was varied in these experiments was $-\Delta$, or the depth of slide submergence. A list of the particular submergences used in the experiments can be seen in the table 3.3. All but one of the submergences were determined from the Liu et al. work, the other was chosen to be slightly deeper then the deepest slide used by Liu et al. in order to calculate a fuller range of results.

Table 3.3: List of depths of submergence $-\Delta$ used in numerical simulations.

-Δ
0.047 m
0.095 m
0.143 m
0.190 m
0.286 m
0.405 m
0.501 m
0.600 m

In addition to these two variables, the rigidity of the slide was considered. The rigidity was controlled by fixing the viscosity of the slide material. For the set of experiments conducted here the viscosity was set to that of water, 1 cP. The rationale behind was to conduct an initial set of experiments with slides of virtually no yield strength in order to understand the effect that the rigidity of the slide has on the results.

3.3 Data analysis

iSALEplot, iSALE's data processing program, and customized Python scripts are employed for the analysis of the data. The overall data analysis consisted of measuring the cavity dynamics of the slide, the runup and effectively determining relationships between the selected parameters. Figure 3.2 shows a graphical representation of the modeling that was conducted for the present research.

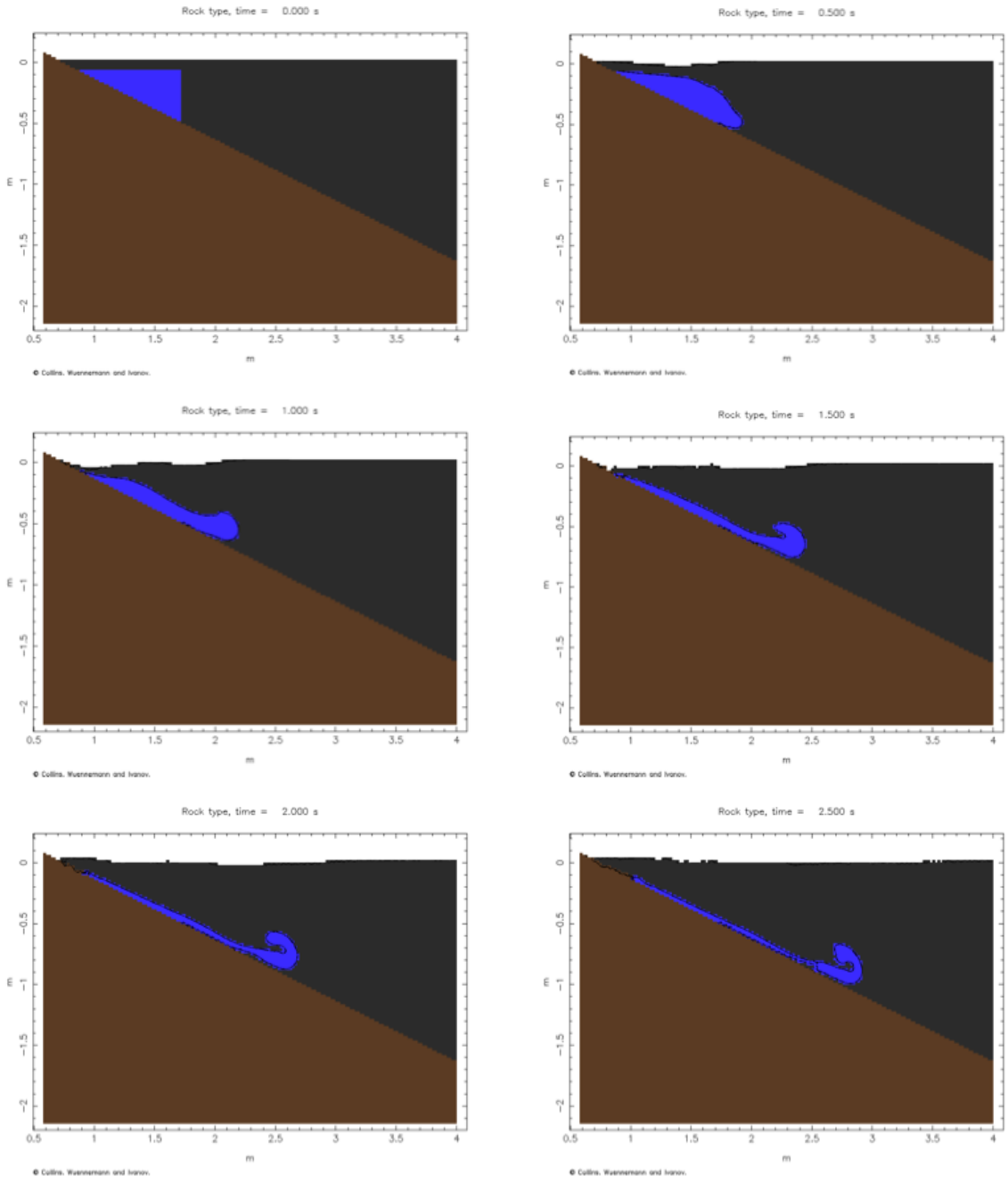

Fig. 3.2.: Snapshots illustrating slide motion at $t = 0.0$s to $t = 2.50$s, slope is in brown, slide blue and water in black.

3.3.1 Cavity dynamics analysis

The cavity, is defined as the air filled area created above the slide between the free surface at $t = 0$ and free surface at later times. This area is created by pressure imbalances generated by the downward movement of the slide. The evolution of this area is depicted in figure 3.3a.

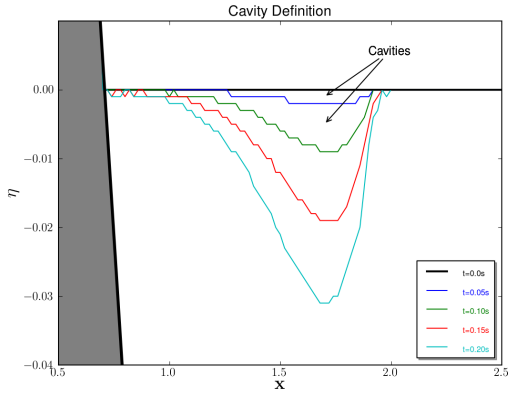

(a) Cavity example for four different times.

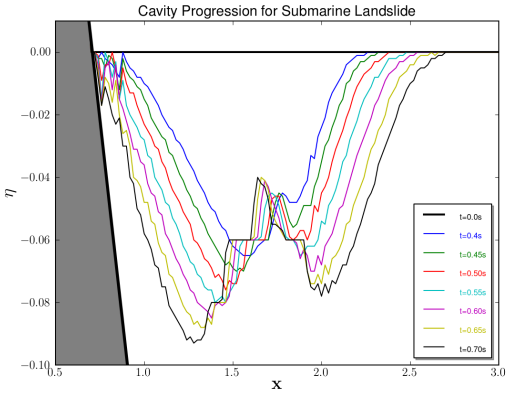

(b) Cavity evolution from 0.0s to 0.70s.

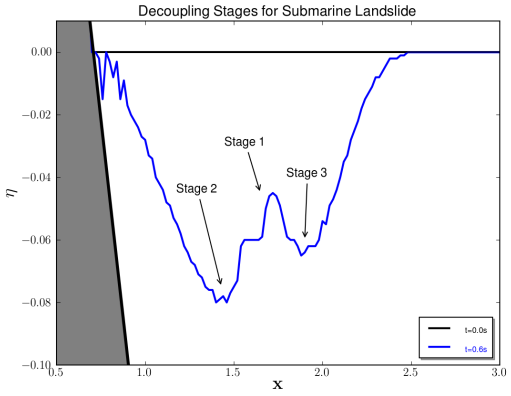

(c) Cavity decoupling stages

Fig. 3.3.: Cavity definition and evolution for a submarine landslide. The abscissa represents horizontal distance, x and the ordinate η is wave height. The 355kg slide with a submergence depth of $-\delta$ =1.935m was used to create these images.

Figure 3.3a and figure 3.6a are examples of the evolution of the free surface within the first second of slide motion. In figure 3.3a in can be observed that as time

progresses the free surface is moving downward and produces a larger cavity. The minimum of the free surface, measured orthogonally from the free surface at $t = 0.0s$, likewise increases as time increases. In comparison a more elaborate process can be observed in figure 3.6a. The cavity is no longer uniformly changing, and the points on the free surface are starting to change direction. This change of direction is not uniform for all points on the free surface and starts to occur in the center of the cavity first. The point in time during which the first point starts to change direction is defined as the stage one separation time, τ_1, and the distance measured orthogonally from the the free surface to that point is distance at time τ_1, S_{τ_1}. Stage 2 occurs between stage 1 and the shoreline and occurs when S_{τ_2} is maximized. Stage 3 occurs seaward from stage 1.

The stages are labeled in figure 3.3c. It is the authors contention that the time at which stage three occurs the slide is no longer transferring energy to the water column that will effect the wave formation and propagation. Therefore from time zero to, τ_3 will be the calculated interval during which the slide properties are affecting the water column. Specifically this will be the time interval during which the slide's geometric parameters are affecting the water column and the deformability of the slide is critical. It is further believed that the stage 2 separation time is the period during which the slide parameters are going to effect the near shore propagating wave, and therefore for this study this is the stage of interest.

Two methods have been employed to determine τ_2. The first method involves calculating the rate change of area over time such that the rate change of area is less then zero $t = \tau_2$.

$$\frac{da}{dt} < 0 : t = \tau_2 \tag{3.1}$$

Initially the entire free surface was taken into account for this calculation since and since $S_{\tau_2} > S_{\tau_3} > S_{\tau_1}$ it was believed that this would lead to and accurate result. However it actually lead to incorrect results when compared to visual inspection of

the a graphical output of the experiment. This was because the width of the cavity grows at a rate, such that the maximum area occurs not at one of the separation times.

Therefore forty-five cells were selected directly above the slide in order to calculate this value, which correlates to the length of the slide (b=0.9144 m). These values were selected because upon visual inspection of the experiment the τ_2 decoupling occurs within the range of cells above the slide. The results of this can be seen in the upper graph in figure 3.4. For this particular case τ would be defined to be around 0.8 seconds.

The second method that has been implemented to determine τ_2 employs using the rate of change of S over time to select τ. The argument is similar the volume method described above i.e.:

$$\frac{dS}{dt} < 0 : t = \tau, \tag{3.2}$$

where S is the length of a vector projected orthogonally from the water surface at $t = 0.0s$ to the minimum on the water surface in future times. Currently this method appears to give a more reasonable value for τ_2. An example of this calculation is given in the lower graph of figure 3.4.

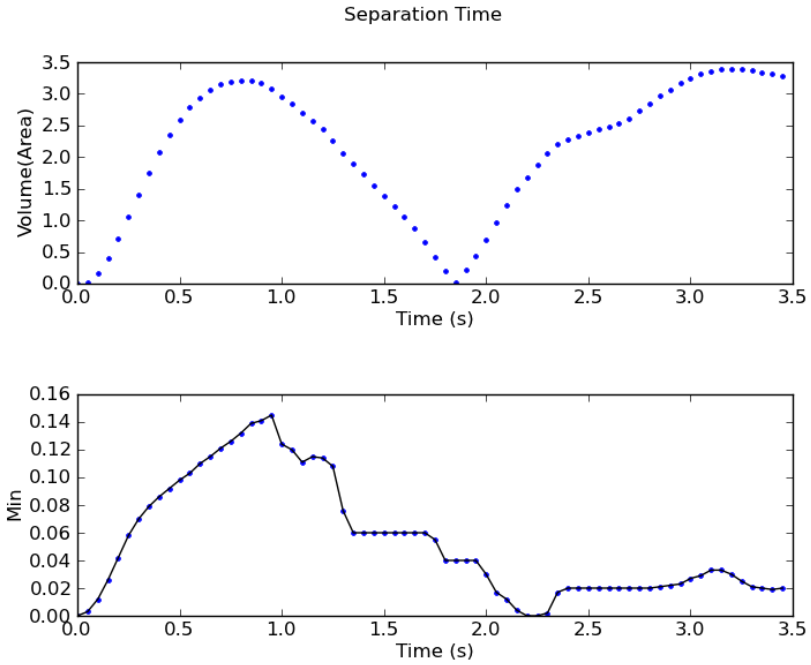

Fig. 3.4.: The upper graph is an example of the area calculation and the lower is an example of the calculation of S for the 355.0 kg, $-\Delta$ =0.047m slide.

Logically the slide is going to transfer energy into the water as it evolves. In unrealistic, but simple, circumstances this would be a complete transfer of energy as in all of the initial potential energy from the slide would be converted to kinetic energy of the water i.e:

$$\frac{dE_s}{dt} = -\frac{dE_w}{dt} \tag{3.3}$$

However, not all of the energy is converted from the slide to the kinetic energy in the water, with effects such as the internal frictional energy losses due to slide deformation prevent this transfer from being one to one. Therefore the author is introducing a variable $\kappa = \kappa(t)$ that represents the incremental energy transfer over time. κ therefore would reflect the amount of energy conversion that takes place during the slides evolution. Note that $\kappa \in [0, 1]$.

$$\frac{dE_s}{dt} = -\kappa \frac{dE_w}{dt} \tag{3.4}$$

Figure 3.5 is the predicted relationship between κ and time. The line from A to B is where the slide is fully coupled to the free surface and transferring the maximum amount of incremental energy. B to C represents stage 1 where the slide has undergone the initial decoupling, C to D the second stage of decoupling has begun, D to E the third stage, and E to F the slide has decoupled from the free surface and the amount amount of conversion is going to zero. Point C would represent stage 1 decoupling, D stage 2 decoupling and E stage 3 decoupling. Where after point D κ would only be contributing to the seaward propagating wave.

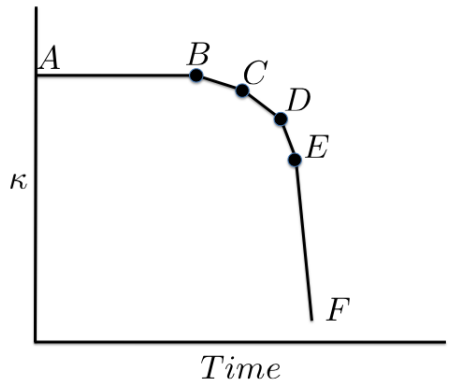

Fig. 3.5.: Diagram of how κ the energy transfer parameter changes over the time during the coupling of the slide. From A to B the slide is fully coupled to the free surface and transferring the maximum amount of energy. From B to C represents stage 1 where the slide has undergone the initial decoupling, C to D the second stage of decoupling has begun, D to E the third stage, and E to F the slide has decoupled from the free surface and the amount amount of conversion is going to zero. C would represent stage 1 decoupling, D stage 2 decoupling and E stage three decoupling.

If one was able to then determine the time during which these stages occurred one would be able to determine the incremental contribution of κ over time. This work will focus on determining τ_2 which will give insight into the amount of time during which the energy from the slide is being converted into the shoreward propagating wave and will allow a determination of the period during which the slides parameters are important in the slide-water column relationship.

3.3.2 Runup analysis

The runup of the near-field wave is also analyzed and compared to figure 2.10. This is done by analyzing the free surface points for all times after they are extracted from runs via iSALEPlot. They are then read into a personalized script and the intersection between the water surface and slope will be calculated. A number of approaches was used to extrapolate the values between the slope and the closest few data points, with a linear fit per Lynett and Liu (2002) being decided upon. In this paper the authors linearly fit a line to the to points nearest to the shore and defined the intersection of this line and the shore as the runnup. This can be seen in figure 3.6. The results from this analysis are then plotted against figure 2.10.

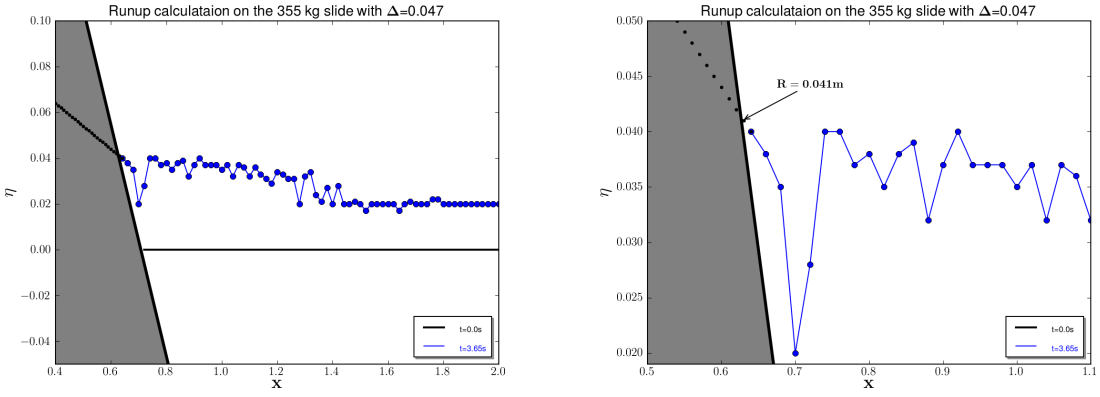

(a) Runup calculation example.

(b) Runup calculation exampled zoomed in.

Fig. 3.6.: Runup measurement example.

3.3.3 Modeling concerns

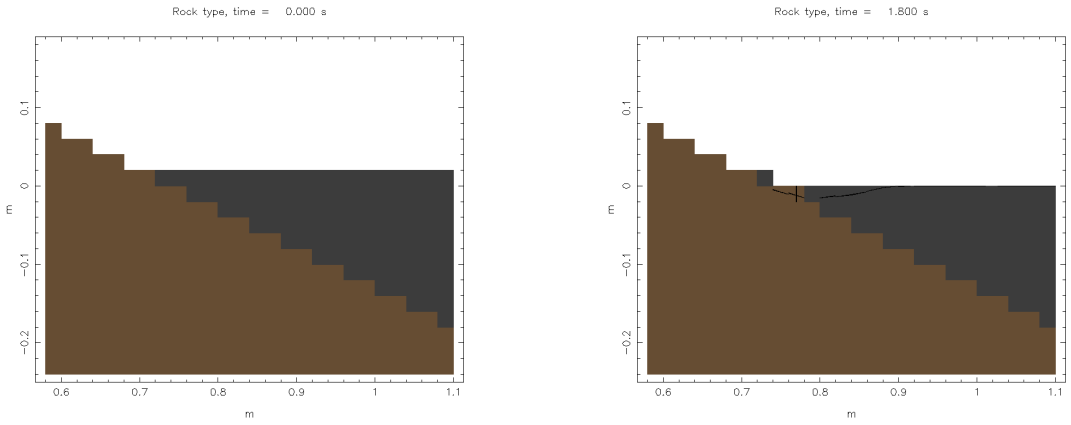

Fig. 3.7.: Snapshots illustrating wave motion at $t = 0.0$s and $t = 1.80$s, slope is in brown, and water is in black. Notice the cell filled with water for the $t = 1.80$s snapshot.

The grid size, 0.02m, was chosen in order to increase the speed of the calculation, however to accurately model runups on this scale it is was found that a much smaller gird size is necessary. One issue can be seen in the effect that the grid size has on the ability for water to runup the slope. It appears that upon visual inspection the water in some situations gets walled up behind a grid cell. An example of this can be seen in figure 3.8. These are time slices from iSALEPlot of 190.0kg, $\nu = 0$cP, and $-\Delta = 0.60$m model run. The particular times can be seen at the top of each picture and span from 0.0s to 2.8s.

The second observation to note is that these images can be seen with the water filled cell located at x=0.75m and y=0.0m on the 1.70s time slice. This cell contains water yet it has been completely separated from the water column. This separation has lead to difficulties in calculating an accurate intersection between the slope and the water column with the data that can currently be extracted from via iSALEPlot.

The third observation to note was the effect that the grid cell has in preventing the water from moving up the slope. This can been seen in the time slices occurring between 1.90s-2.05s. During this time the water should be moving up the slope however it does not appear to have enough energy during this time interval to overcome the forces that the slope filled grid cell is exerting on the water column.

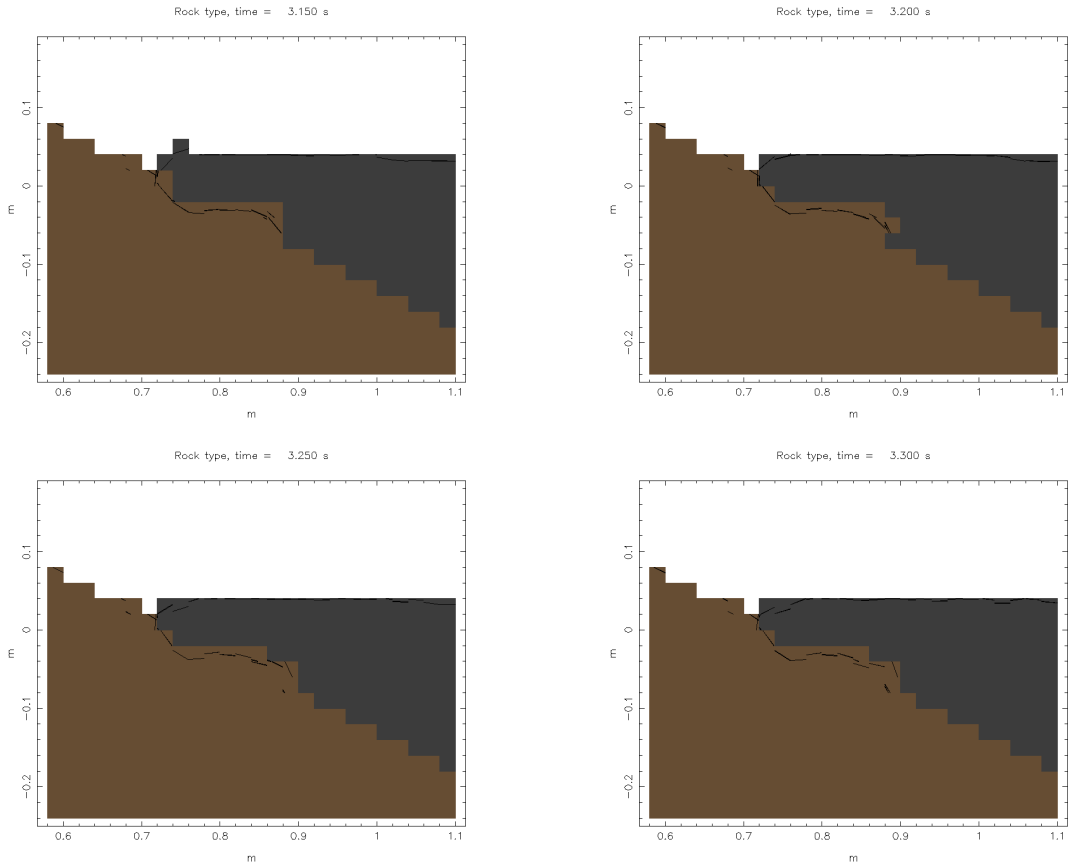

Fig. 3.8.: Snapshots illustrating wave motion at $t = 3.15$s to $t = 3.30$s, slope is in brown, and water is in black. Notice the that the intersection of slope and water stays in the same grid cell for all times.

The fourth thing to note is observed in the lowest two time histories. Very complex morphodynamic behavior can be observed near the intersection of the water surface and the slope. This behavior needs to be examined in more detail and

determined if it is geologically realistic. Since the goal is to extract the runup from these runs and compare it was laboratory experiments where the slope was unable to deform it is crucial to be able to determine how much wave energy is lost in this process.

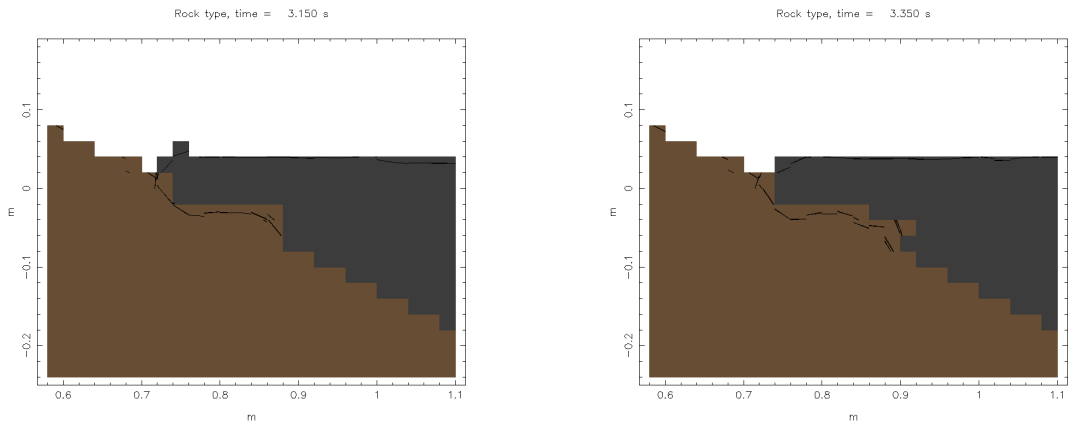

Fig. 3.9.: Snapshots illustrating wave motion at $t = 3.15$s and $t = 3.35$s, slope is in brown, and water is in black. Notice the morphodynamic behavior of the slope below the water slope interface.

4. RESULTS

4.1 Cavity dynamics and separation time

The cavity dynamics of forty runs were analyzed and the separation time at stage 2, τ_2, was calculated. These runs consisted of five difference masses, table 3.2, and eight different depths of submergence, table 3.3. The nondimensionalized depth of submergence, Δ divided by slide length b and specific gravity γ verses τ_2 was then plotted, figure 4.1.

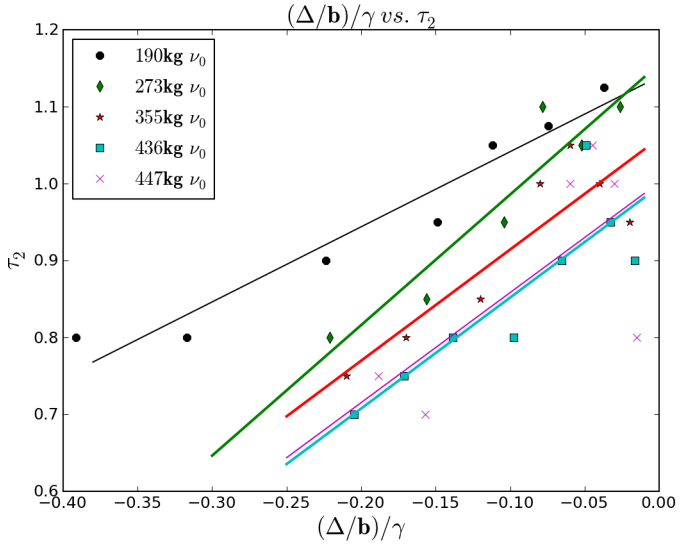

Fig. 4.1.: Depth of submergence verses stage two separation time and corresponding linear fits. τ_2 is the separation time, Δ the depth of submergence, b slide length, and γ specific gravity of the slide. See table 4.1 for closeness of fit calculations.

A linear regression was fit to the points. For an accuracy comparison r^2 was calculated and is listed in table 4.1. Those these points have a strong r^2 correlation coefficient, it is not entirely clear that they have a linear relationship. This can be seen in figure 4.2, where a line is plotted to the points.

Table 4.1: Table of r^2 values for linear regression conducted on data collected from initial model runs. Calculations correspond to figure 4.1.

$190.0kg\ \nu_0$	$r^2 = 0.94$
$273.0kg\ \nu_0$	$r^2 = 0.89$
$355.0kg\ \nu_0$	$r^2 = 0.78$
$436.0kg\ \nu_0$	$r^2 = 0.74$
$447.0kg\ \nu_0$	$r^2 = 0.47$

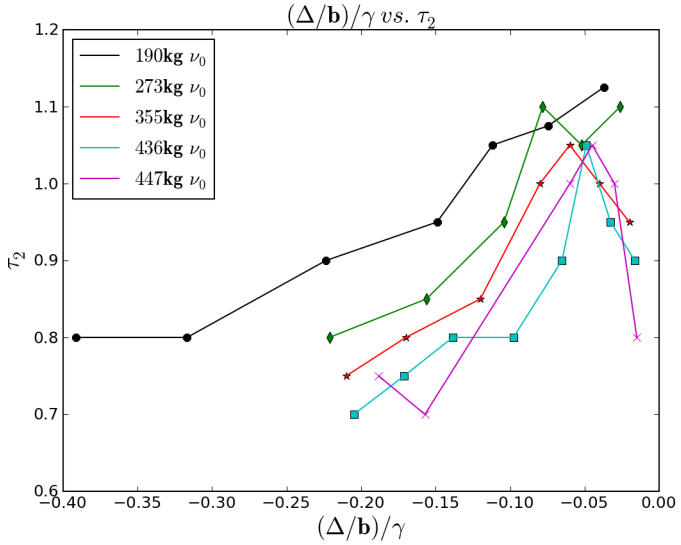

Fig. 4.2.: Depth of submergence verses stage two separation time. τ_2 is the separation time, Δ the depth of submergence, b slide length, and γ specific gravity of the slide.

In figure 4.2 a general shape can be discerned from the lines. This shape resembles a negatively skewed distribution with a maximum between -0.10 and 0.0 $(\Delta/b)/\gamma$.

This leads one to believe that for values of Δ near zero there is potentially a different relationship then the relationship slides at greater depths.

An exponential relationship can be seen when instead of plotting the separation time at stage 2, the vector length S_{τ_2} is plotted against nondimensionalized depth of submergence. In can still be seen though that for smaller depths of submergence, is inconsistency in the relationship. This leads to the belief that for smaller depths of submergence the surface tension of the water plays a larger role in the wave and cavity formation then for slides at greater depths. It is also possible that this irregularity in the data could be based solely on the current grid spacing and that a much finer grid is necessary in order to solidify the results further.

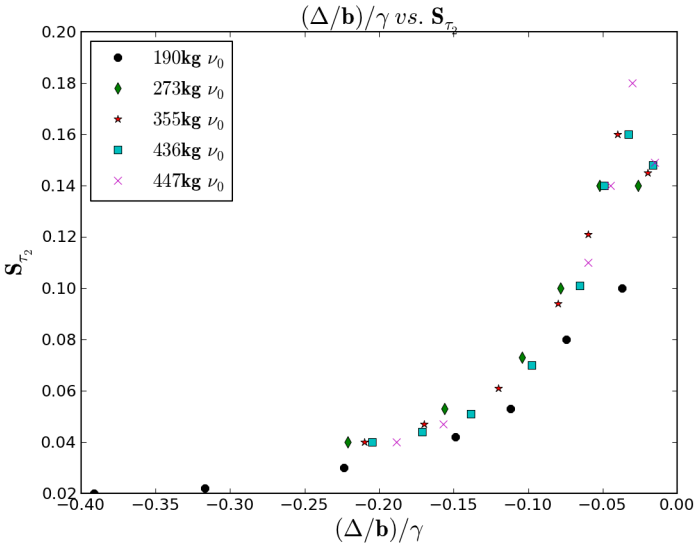

Fig. 4.3.: Depth of submergence verses s_{τ_3}, measured orthogonally from free surface at $t = 0$s.

4.2 Runup

The data plotted as circles and diamonds, in figure 4.4 was taken from the results of the Liu et al. (2005) experiments. The circles represent experiments from series

A, and the diamonds from series B. The squares points is data from the simulations that were run with iSALE. This graph depicts the relationship between nondimensionalized depth of submergence and nondimensionalized runup. There are currently eleven cases presented here from two masses, 190.0kg and 355.0kg.

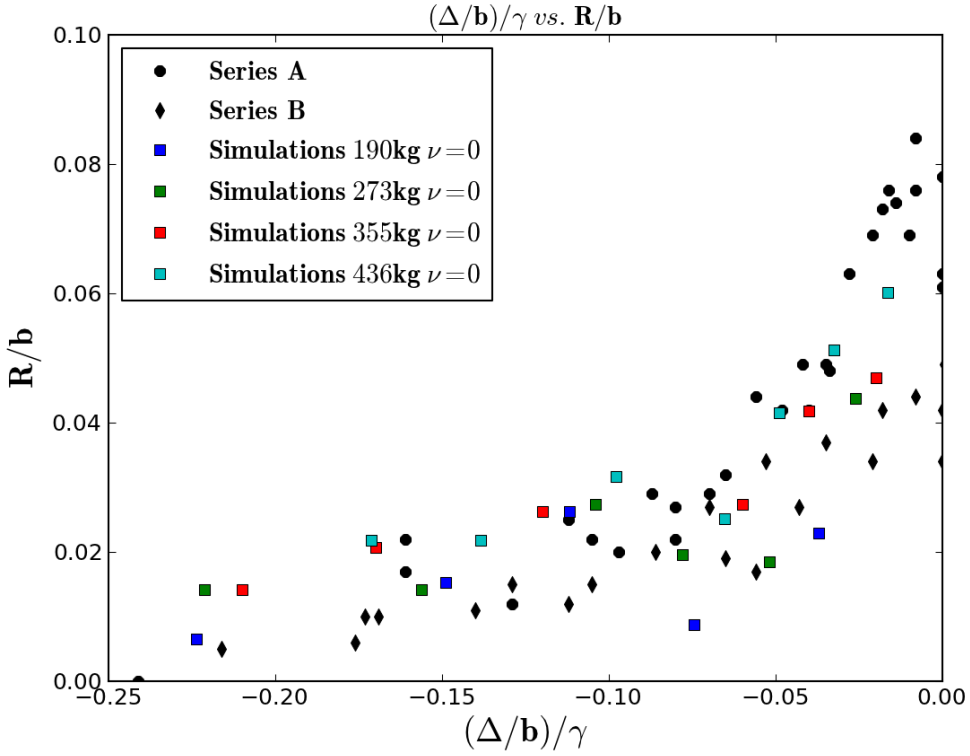

Fig. 4.4.: Liu et al. (2005) nondimensionalized runup versus depth of submergence with with simulations plotted from iSALE for slides of zero viscosity.

The overall trend of the data is what was expected, but due to the grid size and unforeseen numerical idiosyncrasies the accuracy of the points is suspect. The runnup values were calculated by taking the two points of the free surface that were the closest to the slope and linearly extrapolating those points to the slope, with the runup being measured as the intersection. This in some cases gave values that could

be unrealistic, since small changes in the y-axis variation of the points could case large changes in the projected value since the grid spacing was so large.

5. CONCLUSION

5.1 Research impact

One of the primary goals of this study is to cultivate a higher level of understanding of submarine landslide induced tsunamis. This research is needed for risk assessment and hazard mitigation of the potentially destructive event. The introduction of the state-of-the-art hydrocode iSALE as numerical tool for this type of research will allow for the testing of wide ranges of parameters in order to better facilitate focused laboratory studies and allow for a quantifiable analysis of many simulations that are impossible to run in the laboratory. Below each of the previous objectives will be listed and the degree to which the objective was met and the impact that is has will be described.

1. Are there any differences between runup heights generated from deformable submarine landslides and solid slides of the same geometry? How critical is the deformability of the slide in generating the wave height?

    - Results & Impact - Although the data is inconclusive at the current juncture, there appears to be an overall trend of lower runup values for deformable slides with low viscosity. It is the author's belief that this will be further proved with more model runs at a higher resolution. It is also the author's belief that the runup of these slides will increase with increasing viscosity, but that also will take more runs to prove. In answering these questions the author hopes to determine the relative importance of conducting computationally intensive numerical experiments and difficult, not to scale, laboratory experiments with deformable submarine slides. In all of the runs, it was observed that decoupling occurred at some point after significant deformation occurred. It is therefore reasonable to believe that deformability is critical in accurately modeling these events.

2. Are we able to accurately quantify the amount of time during which energy is transferred from the slide body to generate free surface deformation? What slide parameters effect this relationship?

    - Results & Impact - If the amount of time during which the energy from the slide is transferred can be quantified it will allow for a quantification of the amount of time during which the material and geometric parameters of the slide contribute to free surface deformation. For the cases analyzed this time was able to be accurately determine and a strong linear correllation was found between depth of submergence and separation time. Energy calculations however are still needed in order to determine if this is actually the time during which no more energy is being converted to wave energy involved in the surface waveforms generated. With the initial models a unique depth interval was identified during which the slide better coupled with the water column. More runs will need to be conducted to elucidate this but if this is the case it will determine a range of depths over which a greater amount of wave energy can be generated. A understanding of this will help immensely in assessing the risk that these events could have on coastlines.

3. What effects do the viscosity, mass, and depth of submergence have on the generated run up for fully deformable slides? To what degree do each of the parameters effect this value?

    - Results & Impact - Understanding the parametric relationship between viscosity, mass, depth of submergence , and runup will help with quantifying the risk associated with different types of these events. To the authors knowledge a parametric study including the viscosity ("simulated yield strength") of this type has not been conducted. Further runs will

need to be conducted in order to determine any significant relationships between these events other then was has already been described above.

In conclusion, much work is still needed in analyzing the relationship between submarine landslides and wave generation. More model runs will need to be conducted at a higher resolution in order to accurate analyze the parameter relationships between the slide properties and water wave generation.

Fair is what we see, Fairer what we have perceived, Fairest what is still in veil.
-Anatomist and geologist Nicolaus Steno, 1673

REFERENCES

Altinok, Y., S. Tinti, B. Alpar, A. Yalciner, S. Ersoy, E. Bortoluci, and A. Armigliato, 2001, The tsunami of August 17, 1999 in Izmit Bay, Turkey: Natural Hazards, **24**, 133–146.

Amsden, A., H. Ruppel, and C. Hirt, 1980, SALE: A simplified ALE computer program for fluid flow at speeds: Los Alamos National Laboratories Report LA-8095, 101.

Anderson, C., 1987, An overview of the theory of hydrocodes: International Journal of Impact Engineering, **5**, 33–59.

Asari, Y., Y. Koido, K. Nakamura, Y. Yamamoto, and M. Ohta, 2000, Analysis of medical needs on day 7 after the tsunami disaster in Papua New Guinea: Prehospital Disaster Med., **15**.

Bardet, J., C. Synolakis, H. Davies, F. Imamura, and E. A. Okal, 2003, Landslide tsunamis: Recent findings and research directions: Pure and applied geophysics, **160**, 1793–1809.

Ben-Menahem, A., and M. Rosenman, 1972, Amplitude patterns of tsunami waves from submarine earthquakes: Journal of Geophysical Research, **77**, 3097–3128.

Bohannon, R. G., and J. V. Gardner, 2004, Submarine landslides of San Pedro Escarpment, southwest of Long Beach, California: Marine geology, **203**, 261–268.

Borrero, J., C. Synolakis, and H. Fritz, 2006, Northern Sumatra field survey after the December 2004 great Sumatra earthquake and Indian Ocean tsunami: Earthquake spectra, **22**, 93–104.

Borrero, J., R. Weiss, E. Okal, R. Hidayat, Suranto, D. Arcas, and V. V. Titov, 2009, The tsunami of 2007 September 12, Bengkulu province, Sumatra, Indonesia: posttsunami field survey and numerical modelling: Geophysics Journal International, **178**, 180–194.

Borrero, J. C., 2002, Tsunami hazards in Southern California: Ph.D. Thesis-University of Southern California, 220.

Borrero, J. C., J. F. Dolan, and C. E. Synolakis, 2001, Tsunamis within the eastern Santa Barbara Channel: Geophysics Research Letters, **28**, 643–646.

Bourgeois, J., C. Petroff, H. Yeh, V. Titov, C. Synolakis, B. Benson, J. Kuroiwa, J. Lander, and E. Norabuena, 1999, Geologic setting, field survey and modeling of the Chimbote, northern Peru, tsunami of 21 February 1996: Pure and Applied Geophysics, **154**, 513–540.

Capone, T., A. Panizzo, and J. Monaghan, 2010, SPH modelling of water waves generated by submarine landslides: Journal of Hydraulic Research, **48**, 80–84.

Collins, G., H. Melosh, and B. Ivanov, 2004, Modeling damage and deformation in impact simulations: Meteoritics & Planetary Science, **39**, 217–231.

de Ballore, F. M., 1907, La science seismologique: A. Colin, Paris.

DeLange, W., and Moon, 2004, Estimating earthquake and landslide tsunami hazard for the new zealand coast: Bulletin of the New Zealand Society for Earthquake Engineering, **37**, 62–69.

Eissler, H. K., and H. Kanamori, 1987, A single-force model for the 1975 Kalapana, Hawaii, earthquake: Journal Geophysics Research, **92**, 4827–4836.

Fritz, H., 2002, Initial phase of landslide generated impulse waves: Ph.D. Dissertation to the Swiss Federal Institute of Technology Zurich, **ETH No. 14871**.

Fritz, H., W. Hager, and H. Minor, 2003a, Landslide generated impulse waves. I. Instantaneous flow fields: Experiments in fluids, **35**, 505–519.

———, 2003b, Landslide generated impulse waves. II. Hydrodynamic impact craters: Experiments in fluids, **35**, 520–532.

———, 2004, Near field characteristics of landslide generated impulse waves: Journal of Waterway, Port, Coastal, and Ocean Engineering, **130**, 287–302.

Fritz, H. M., 2000, PIV applied to landslide generated impulse waves: 10th Intl. Symp. on Applications of Laser Techniques to Fluid Mechanics, 1–12.

Fritz, H. M., W. Hager, and H. Minor, 2001, Lituya bay case: Rockslide impact and wave run-up: Science of Tsunami Hazards the International Journal of the Tsunami Socitey, **19**, 3–22.

Fryer, G., P. Watts, L. Pratson, and J. Gardner, 2001, The tsunami of 1 April 1946: A landslide in the upper forearc: Prediction of underwater landslide hazards. Rotterdam, Balkema press.

Fryer, G., P. Watts, and L. F. Pratson, 2004, Source of the great tsunami of 1 April 1946: a landslide in the upper Aleutian forearc: Marine geology, **203**, 201–218.

Fujii, Y., K. Satake, S. Sakai, M. Shinohara, and T. Kanazawa, 2011, Tsunami source of the 2011 off the Pacific coast of Tohoku, Japan earthquake: Earth Planets Space.

Galanopoulos, A., 1956, The seismic sea-wave of July 9, 1956: Proc. Acad. Athens, **82**, 90–101.

Geist, E., 2000, Origin of the 17 July 1998 Papua New Guinea tsunami: Earthquake or landslide: Seismological Research Letters, **71**, 344–351.

———, 2001, Reply to comment by EA Okal and CE Synolakis on" Origin of the 17 July 1998 Papua New Guinea tsunami: Earthquake or landslide?": Seismological Research Letters, **72**, 367–372.

Geist, E., V. Titov, D. Arcas, F. Pollitz, and S. Bilek, 2007, Implications of the 26 December 2004 Sumatra–Andaman earthquake on tsunami forecast and assessment models for great subduction-zone earthquakes: Bulletin of the Seismological Society of America, **97**, 249–270.

Gisler, G., and R. Weaver, 2006, SAGE calculations of the tsunami threat from La Palma: Science Tsunami Hazards, **24**, 295.

Gisler, G., R. Weaver, C. Mader, and M. Gittings, 2003, Two and three dimensional simulations of ocean impacts: Science of Tsunami Hazards-LANL Report, **LA-UR 02-66-30**.

Gisler, G. R., R. P. Weaver, C. L. Mader, and M. Gittings, 2004, Two-and three-dimensional asteroid impact simulations: Computing in Science & Engineering, 46–55.

Goff, J., L. Philip, B. Higman, R. Morton, B. Jaffe, H. Fernando, P. Lynett, H. Fritz, C. Synolakis, and S. Fernando, 2006, Sri Lanka field survey after the December 2004 Indian Ocean tsunami: Earthquake spectra, **22**, S155.

Grilli, S., S. Vogelmann, and P. Watts, 2002, Development of a 3D numerical wave tank for modeling tsunami generation by underwater landslides: Engineering analysis with boundary elements, **26**, 301–313.

Grilli, S., and P. Watts, 2005, Tsunami generation by submarine mass failure. I: Modeling, experimental validation, and sensitivity analyses: Journal of Waterway, Port, Coastal, and Ocean Engineering, **131**.

Gutenberg, B., 1939, Tsunamis and earthquakes: Bulletin of the Seismological Society of America.

Hammack, J., 1973, A note on tsunamis: Their generation and propagation in an ocean of uniform depth: J. Fluid Mech., **60**, 769–799.

Hampton, M., H. J. Lee, and J. Locat, 1996, Submarine landslides: Reviews of Geophysics.

Hasegawa, H., and H. Kanamori, 1987, Source mechanism of the magnitude 7.2 Grand Banks earthquake of November 1929: Double couple or submarine landslide?: Bulletin of the Seismological Society of America, **77**, 1984–2004.

Heinrich, P., 1992, Nonlinear water waves generated by submarine and aerial landslides: Journal of Waterway, Port, Costal, and Ocean Engineering, **118**, 249–266.

Heinrich, P., A. Piatanesi, E. A. Okal, and H. Hebert, 2000, Near-field modeling of the July 17, 1998 tsunami in Papua New Guinea: Geophys. Res. Lett, **27**, 3037–3040.

Heller, V., 2008, Landslide generated impulse waves: Prediction of near field characteristics: eprints.soton.ac.uk.

Imamura, F., E. Gica, T. Takahashi, and N. Shuto, 1995, Numerical simulation of the 1992 Flores tsunami: Interpretation of tsunami phenomena in Northeastern Flores Island and damage at Babi Island: Pure and applied geophysics, **144**.

Ivanov, B., 2005, Numerical modeling of the largest terrestrial meteorite craters: Solar System Research, **39**, 381–409.

Ivanov, B., and N. Artemieva, 2002, Numerical modeling of the formation of large impact craters: Catastrophic events and mass extinctions: Impact and beyond-Geological Society of America, **Special Paper 356**, 619–630.

Ivanov, B., D. Deniem, and G. Neukum, 1997, Implementation of dynamic strength models into 2D hydrocodes: Applications for atmospheric breakup and impact cratering: International Journal of Impact Engineering, **20**, 411–430.

Ivanov, B., and A. Deutsch, 1999, Sudbury impact event: Cratering mechanics and thermal history: Large meteorite impacts and planetary evolution II-Geological Society of America, **Special Paper 339**, 389–397.

Jiang, L., and P. LeBlond, 1992, The coupling of a submarine slide and the surface waves which it generates: Journal of Geophysical Research, **97**, 12731–12744.

Jiang, L., and P. H. LeBlond, 1993, Numerical modeling of an underwater bingham plastic mudslide and the waves which it generates: Journal of Geophysical Research, **98**, 10303–10317.

Johnson, W. E., and C. E. Anderson, 1987, History and application of hydrocodes in hypervelocity impact: International Journal of Impact Engineering, **5**, 423–439.

Kanamori, H., 1972, Mechanism of tsunami earthquakes: Physics of the Earth and Planetary Interiors, **6**, 346—35.

Kawata, Y., B. Benson, J. Borrero, H. Davies, W. DeLange, F. Imamura, H. Letz, J. Nott, and C. Synolakis, 1999, Tsunami in Papua New Guinea was as intense as first thought: EOS Transactions American Geophysical Union, **80**, 104–105.

Kikuchi, M., Y. Yamanaka, K. Abe, and Y. Morita, 1999, Source rupture process of the Papua New Guinea earthquake of July 17, 1998 inferred from teleseismic body waves: Earth Planets Space, **51**, 1319–1324.

LeBlond, P. H., and A. T. Jones, 1995, Underwater landslides ineffective at tsunami generation: Science of Tsunami Hazards, **13**, 25–26.

Liu, P., P. J. Lynett, and C. E. Synolakis, 2003, Analytical solutions for forced long waves on a sloping beach: J. Fluid Mech., **478**, 101–109.

Liu, P., T. Wu, F. Raichlen, C. Synolakis, and J. C. Borrero, 2005, Runup and rundown generated by three-dimensional sliding masses: J. Fluid Mech., **536**, 107–144.

Locat, J., and H. J. Lee, 2002, Submarine landslides: Advances and challenges: Canadian Geotechnical Journal.

Lynett, P., and P. Liu, 2002, A numerical study of submarine–landslide–generated waves and run–up: Proceedings of the Royal Society Mathmatical, Physical and Engineering Sciences, **458**, 2885–2910.

Lynett, P. J., J. C. Borrero, P. L.-F. Liu, and C. E. Synolakis, 2003, Field survey and numerical simulations: A review of the 1998 Papua New Guinea tsunami: Pure and Applied Geophysics, **160**, 2119–2146.

Mader, C. L., and M. Gittings, 2002, Modeling the 1958 Lituya Bay mega-tsunami, II: Science of Tsunami Hazards, **20**.

Mariotti, C., and P. Heinrich, 1999, Modelling of submarine landslides of rock and soil: International Journal for Numerical and Analytical Methods in Geomechanics, **23**, 35–354.

Matsuyama, M., J. Walsh, and H. Yeh, 1999, The effect of bathymetry on tsunami characteristics at Sisano Lagoon, Papua New Guinea: Geophysical Research Letters, **26**, 3515–3516.

McCulloch, D., 1985, Evaluating tsunami potential, in: Evaluating earthquake hazards in the Los Angeles Region-An earth science perspective: USGS Professional Paper, **1360**, 375–413.

McCurry, J., 2011, Japan: The aftermath: The Lancet, **377**, 1061–1062.

McSaveney, M., J. Goff, D. Darby, P. Goldsmith, A. Barnett, S. Elliott, and M. Nongkas, 2000, The 17 July 1998 tsunami, Papua New Guinea: evidence and initial interpretation: Marine geology, **170**, 81–92.

Melosh, H., 1984, Impact ejection, spallation, and the origin of meteorites: Icarus.

———, 1987, High-velocity solid ejecta fragments from hypervelocity impacts: International Journal of Impact Engineering.

Melosh, H., E. Ryan, and E. Asphaug, 1992, Dynamic fragmentation in impacts: Hydrocode simulation of laboratory impacts: Journal of Geophysical Research.

Meunier, M., 1993, Classification of streams flows: Proceedings of the Pierre Beghin International Workshop on Rapid Gravitational Mass Movements, CEMAGREF, Grenoble, France, 231–236.

Miller, D. J., 1960, The Alaska earthquake of July 10, 1958: Giant wave in Lituya Bay: Bulletin of the Seismological Society of America, **50**, 253–266.

Milne, J., 1898, Earthquakes and other earth movements: Paul, Trench, Trubner & Co., London.

Moscardelli, L., and L. Wood, 2008, New classification system for mass transport complexes in offshore Trinidad: Basin Research, **20**, 73–98.

Murty, T., 1979, Submarine slide-generated water waves in Kitimat Inlet, British Columbia: Journal of Geophysical Research, **84**, 7777–7779.

Newman, A., and E. Okal, 1998, Teleseismic estimates of radiated seismic energy: The E/M 0 discriminant for tsunami earthquakes: Journal of Geophysical Research, **103**, 26885–26898.

Okal, E., 1988, Seismic parameters controlling far-field tsunami amplitudes: A review: Natural Hazards, **1**, 67–96.

———, 2003, Normal mode energetics for far-field tsunamis generated by dislocations and landslides: Pure and applied geophysics.

———, 2004, Comment on" Source of the great tsunami of 1 April 1946: a landslide in the upper Aleutian forearc", by GJ Fryer et al.(Mar. Geol. 203 (2004) 201-218): Marine Geology, **209**, 363–369.

Okal, E., C. Synolakis, G. J. Fryer, P. Heinrich, J. C. Borrero, C. Ruscher, D. Arcas, G. Guille, and D. Rousseau, 2002, A field survey of the 1946 Aleutian tsunami in the far field: Seismological Reseach Letters, **73**, 490–503.

Okal, E. A., G. Plafker, C. E. Synolakis, and J. C. Borrero, 2003, Near-field survey of the 1946 Aleutian tsunami on Unimak and Sanak Islands: Bulletin of the Seismological Society of America, **93**, 1226–1234.

Okal, E. A., and C. Synolakis, 2003, A theoretical comparison of tsunamis from dislocations and landslides: Pure and Applied Geophysics.

Okal, E. A., and C. E. Synolakis, 2001, Comment on" Origin of the 17 July 1998 Papua New Guinea tsunami: Earthquake or landslide?" by EL Geist: Seismological Research Letters, **72**, 362–366.

———, 2004, Source discriminants for near-field tsunamis: Geophysical Journal International, **158**, 899–912.

Pelayo, A. M., and D. A. Wiens, 1992, Tsunami earthquakes: Slow thrust-faulting events in the accretionary wedge: Journal of Geophysical Research, **97**, 15,321–15,33.

Pelinovsky, E., and A. Poplavsky, 1996, Simplified model of tsunami generation by submarine landslides: Physics and Chemistry of the Earth, **21**, 13–17.

Plafker, G., and R. Meyer, 1967, Vertical tectonic displacements in south-central Alaska during and prior to the great 1964 earthquake: Journal of Geoscience, **10**, 53–66.

Prager, E. J., 2000, Furious earth: The science and nature of earthquakes, volcanoes, and tsunamis: books.google.com.

Rzadkiewicz, S. A., C. Mariotti, and P. Heinrich, 1997, Numerical simulation of submarine landslides and their hydraulic effects: Journal of Waterway, Port, Costal, and Ocean Engineering, **123**, 149–157.

Satake, K., J. Bourgeois, K. Abe, K. Abe, Y. Tsuji, F. Imamura, Y. Iio, H. Katao, E. Noguera, and F. Estrada, 1993, Tsunami field survey of the 1992 Nicaragua earthquake: EOS, Trans. Am. Geophys. Union, **74**, 156–157.

Satake, K., and Y. Tanioka, 2003, The July 1998 Papua New Guinea earthquake: Mechanism and quantification of unusual tsunami generation: Pure and applied geophysics, **160**, 2087–2118.

Sauer, F., and R. Wiegel, 1946, Memorandum on laboratory experiments on waves generated by an underwater landslide: Tech. Rep. Dept. of Eng. Univ. of Calif., Berkeley Calif.,, $\mathbf{HE}_1 16 - 218(unpublished), 2$.

Scidmore, E. R., 1896, The recent earthquake wave on the coast of Japan: National Geographic Magazine, **7**, 285.

Stirem, H., and T. Miloh, 1975, Tsunamis induced by submarine slumping off the coast of Israel: Israel Atomic Energy Commission.

Synolakis, C., 1991, Tsunami runup on steep slopes: How good linear theory really is: Natural Hazards, **4**, 221–234.

Synolakis, C., J.-P. Bardet, J. Borrero, H. Davies, E. Okal, E. Silver, S. Sweet, and D. Tappin, 2002, The slump origin of the 1998 Papua New Guinea tsunami: Proceedings: Mathematical, Physical, and Engineering Sciences, **458**, 763–789.

Synolakis, C., F. Imamura, Y. Tsuji, Matsutomi, S. Matsutomi, TINTI, B. Tinti, B. Cook, and M. Ushman, 1995, Damage, conditions of East Java tsunami of 1994 analyzed: EOS, Trans. Am. Geophys. Union, **76 (26)**, 261–262.

Synolakis, C. E., 2003, Tsunamis and seiches-earthquake engineering handbook-chapter9: 1–113.

Tadepalli, S., and C. Synolakis, 1994, The run-up of N-waves on sloping beaches: Proc. R. Soc. Lond. A, **445**, 99–112.

Tanioka, Y., 1999, Analysis of the far-field tsunamis generated by the 1998 Papua New Guinea earthquake: Geophysical Research Letters, **26**, 3393–3396.

Tappin, D., P. Watts, G. McMurtry, Y. Lafoy, and T. Matsumoto, 2001, The Sissano, Papua New Guinea tsunami of July 1998–Offshore evidence on the source mechanism: Marine geology, **175**, 1–23.

Thompson, S., and H. Lauson, 1972, Improvements in the Chart D radiation-hydrodynamic code 3: Revised analytic equation of state: Sandia Laboratories, Albuquerque, New Mexico, **Report SC-RR-71 0714**, 119.

Tillotson, J., 1962, Metallic equations of state for hypervelocity impact: oai.dtic.mil.

Titov, V., and F. Gonzalez, 1997, Implementation and testing of the method of splitting tsunami (MOST) model: NOAA Technical Memorandum ERL PMEL-112.

Titov, V. V., B. Jaffe, F. I. González, and G. Gelfenbaum, 2001, Re-evaluating source mechanisms for the 1998 Papua New Guinea tsunami using revised slump estimates and sedimentation modeling: ITS 2001 Proceedings, **2**, 389–395.

Tsuji, Y., F. Imamura, H. Matsutomi, C. Synolakis, P. Nanang, Jumadi, S. Harada, S. Han, K. Arai, and B. Cook, 1995, Field survey of the east Java earthquake and tsunami of June 3, 1994: Pure Appl. Geophys., **144**, 839–854.

Verbeck, R., 1900, Kort verslag over de aard-en zeebeving op Ceram, den 30. September 1899: Natuurkund. Tijdschr. voor Ned.-Indie, **60**.

Walder, J., P. Watts, O. E. Sorensen, and K. Janssen, 2003, Tsunamis generated by subaerial mass flows: J. Geophys. Res, **108**.

Ward, S., 1980, Relationships of tsunami generation and an earthquake source: J. Phys. Earth, **28**, 441–474.

———, 1981, On tsunami nucleation. 1. A point source: Journal of Geophysical Research, **86**, 7895–7900.

———, 1982, On tsunami nucleation: II. An instantaneous modulated line source: Physics of the Earth and Planetary Interiors, **27**, 273–285.

———, 2001, Landslide tsunami: Journal of Geophysical Research.

Ward, S. N., and S. Day, 2001, Cumbre Vieja volcano—potential collapse and tsunami at La Palma, Canary Islands: Geophys. Res. Lett.

———, 2003, Ritter Island volcano—lateral collapse and the tsunami of 1888: Geophysical Journal International, **154**, 891–902.

Watts, P., 1997, Water waves generated by underwater landslides: Ph.D. Thesis, California Institute of Technology, 1–318.

———, 1998, Wavemaker curves for tsunamis generated by underwater landslides: Journal of Waterway, Port, Costal, and Ocean Engineering, **124**, 11.

Watts, P., and J. C. Borrero, 2001, Probability distributions of landslide tsunamis: Journal of the International Tsunami Society, **6**, 697–710.

Weiss, R., and H. Bahlburg, 2006, The coast of Kenya field survey after the December 2004 Indian Ocean tsunami: Earthquake Spectra, **22**, S235.

Weiss, R., H. M. Fritz, and K. Wünnemann, 2009, Hybrid modeling of the mega-tsunami runup in Lituya Bay after half a century: Geophysical Research Letters.

Weiss, R., C. E. Synolakis, and J. O'Shay, 2011, Initial waves from deformable submarine landslides: Proceedings of 2011 NSF Engineering Research and Innovation Conference, Atlanta, Georgia, **Grant #0928654**, 1–7.

Weiss, R., and K. Wünnemann, 2007, Large waves caused by oceanic impacts of meteorites: Tsunami and Nonlinear Waves-Springer, Heidelberg, 237–261.

Weiss, R., K. Wünnemann, and H. Bahlburg, 2006, Numerical modelling of generation, propagation and run-up of tsunamis caused by oceanic impacts: model strategy and technical solutions: Geophysical Journal International, **167**, 77–88.

Wiegel, R., 1955, Laboratory studies of gravity waves generated by the movement of a submarine body: Transactions of the American Geophysical Union, **36**, 759–774.

Wunnemann, K., G. Collins, and H. J. Melosh, 2006, A strain-based porosity model for use in hydrocode simulations of impacts and implications for transient crater growth in porous targets: Icarus, **180**, 514–527.

Wünnemann, K., and B. Ivanov, 2003, Numerical modelling of the impact crater depth-diameter dependence in an acoustically fluidized target: Planetary and space science.

Wünnemann, K., and M. Lange, 2002, Numerical modeling of impact-induced modifications of the deep-sea floor: Deep Sea Research Part II, **49**, 969–981.

Wünnemann, K., and J. Morgan, 2005, Is Ries crater typical for its size? An analysis based upon old and new geophysical data and numerical modeling: Large Meteorite Impacts 3-Geological Society of America Special Paper, **384**, 67–83.

Yeh, H., F. Imamura, C. Synolakis, Y. Tsuji, P. Liu, and S. Shi, 1993, The Flores Island tsunami: EOS, Trans. Am. Geophys. Union, **74**, 371–373.